Chapter 5 Sequential Phased Displacement Shear Wall Tests

5.1 Introduction

The five wall configurations described in Section 3.2 were built and tested using the sequential phased displacement (SPD) loading pattern discussed in Section 3.7. Data concerning the load and drift of each wall were used to compute initial and stabilized load resistance, cyclic stiffness, hysteretic energy, potential energy, and the equivalent viscous damping ratio. Equivalent energy, elastic-plastic load deflection curves were fit to the initial cycle and stabilized cycle envelope curves to allow comparisons between monotonic and cyclic response to be made on an equivalent basis. Data concerning movement and performance of the shear walls is discussed, as well as modes of failure and prediction of capacity.

5.2 First Major Event

The first major event (FME), discussed in Section 3.7, is the peak displacement in the first phase of the second displacement pattern in SPD loading. For the first two cyclic tests with Wall A (r = 1.0) and Wall D (r = 0.48), the FME was 1.0 in. (25.4 mm). It was observed that the gypsum board failed before yielding occurred. For this reason, the FME was changed to 0.1 in. (2.54 mm) for the remaining tests of Wall B (r = 0.76), Wall C (r = 0.55) and Wall E (r = 0.30). Wall A (r = 1.0) was repeated with an FME of 0.1 in. (2.54 mm) with minimal reduction in initial and stabilized resistance, indicating that data from Wall A (r = 1.0) and Wall D (r = 0.48) with an FME of 1.0 in. (25.4 mm) could be compared with tests with an FME of 0.1 in. (2.54 mm).

5.3 Property Definitions

Figure 5.1 is used to illustrate displacement as a function of time in one phase of SPD loading (Section 3.7). Points A and B in Figure 5.1 correspond to the peak positive and negative displacement experienced by the wall during the *initial* cycle of one phase of SPD loading. Points C and D in Figure 5.1 correspond to the peak positive and negative displacement resistance experienced by the wall during the final or *stabilized* cycle of one phase of SPD loading. Each phase of SPD displacements was increased by 100% of the FME until catastrophic failure occurred.

Typical initial and stabilized load envelope curves are given in Figure 5. 2. The initial load envelope curve consists of positive and negative peak loads of the first cycle in each phase of SPD loading (i.e. load resistance corresponding to points A and B in in Figure 5.1). The hysteresis and envelope curves for each of the specimens are included in Appendices C - G for reference.

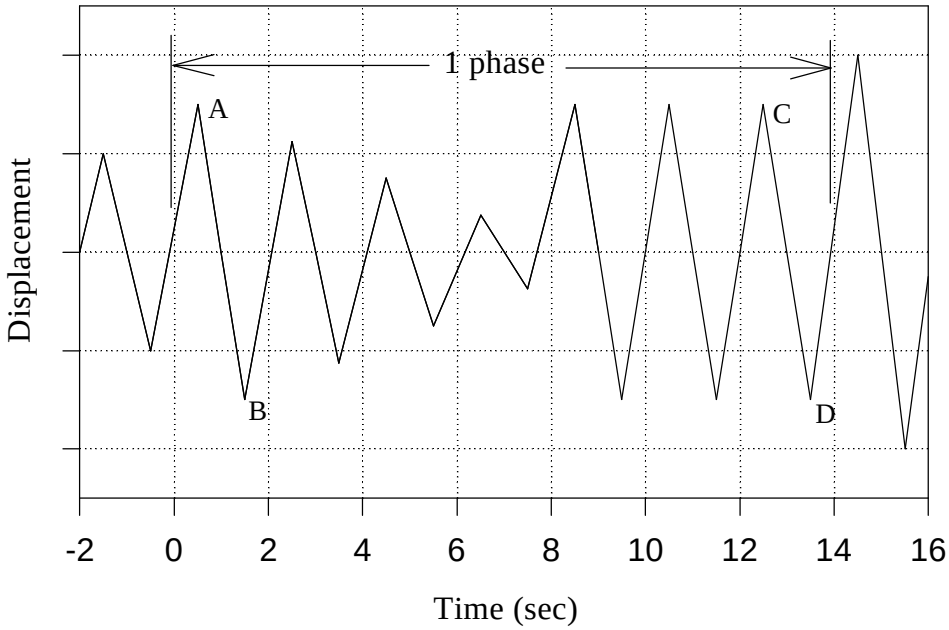

Figure 5. 1- Illustration of displacement in one phase of SPD loading

Data from the initial curve can be used to set design values for shear walls subjected to cyclic loads, but governed by a one time peak load such as wind loading. Data from the stabilized curve can be used to set design values for shear walls subjected to repetitive cycling such as a seismic event. The objectives of design govern which curve, initial or stabilized, should be used.

The average of the peak positive and negative load resisted in the first cycle of a given phase was taken as the initial cycle load resisted at the corresponding interstory drift. The highest average load resistance occurring in the first cycle of each phase during the test was taken as the initial capacity, $F_{max,init}$. Similarly, the highest average load resistance occurring in the last cycle of each phase during the test was taken as the stabilized capacity, $F_{max,stab}$. Interstory drifts corresponding to initial and stabilized capacity were determined and denoted as $\Delta_{max,init}$ and $\Delta_{max,stab}$, respectively.

Load resistance at failure, $F_{failure}$, was determined from the initial and stabilized load envelope curve as the highest load carried by the wall before a significant decrease in load. $\Delta_{failure}$ is defined as the corresponding drift at failure.

Elastic stiffness, k_e, was determined as the slope of the secant between the origin and the point on the load envelope curve corresponding to 40% of F_{max}. Elastic stiffness was determined from both the positive and negative initial load envelope curve and the positive and negative stabilized load envelope curve. Initial and stabilized elastic stiffness was taken as the average stiffness from their respective positive and negative load envelope curves.

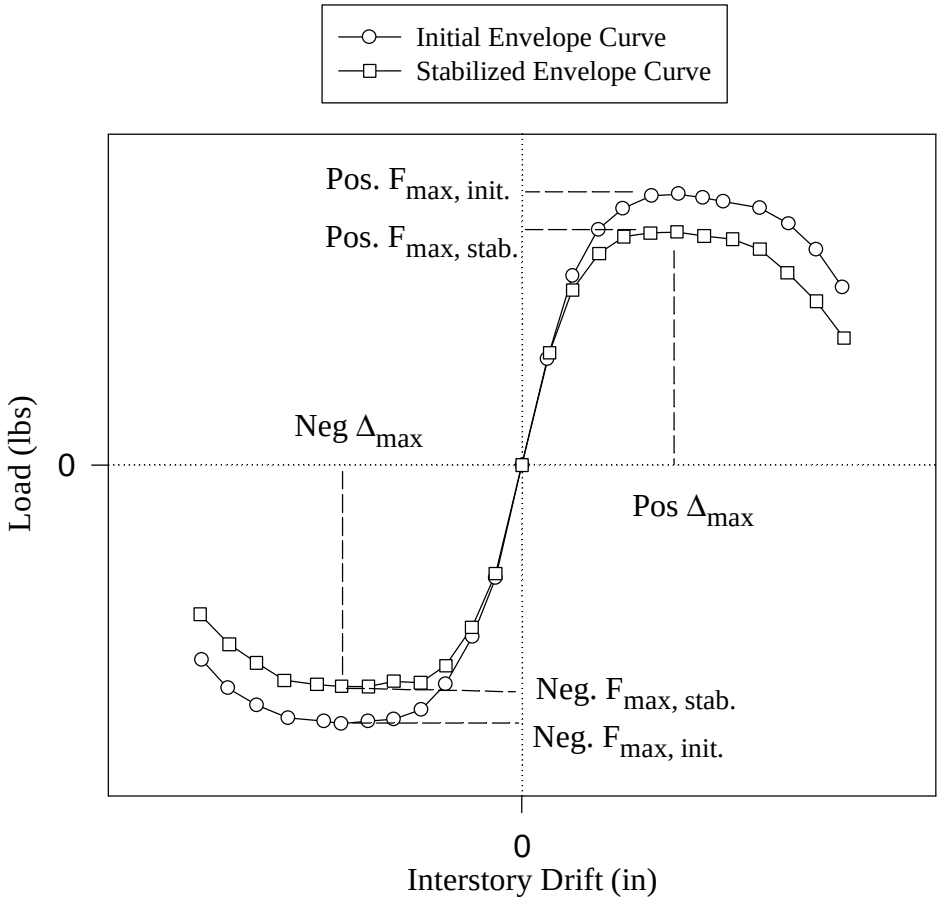

Figure 5. 2- Typical initial and stabilized load-envelope curves

5.3.2 Equivalent Energy, Elastic-Plastic Curve Definitions

Equivalent energy, elastic-plastic curves were determined from the initial and stabilized load envelope curves. This artificial curve, shown in Figure 5.3, depicts how an ideal perfectly elastic - plastic wall would perform and dissipate an equivalent amount of energy. The equivalent elastic-plastic curve (EEPC) was defined so that the area under the EEPC is equal to the area under the load-displacement curve from 0 in. drift to $\Delta_{failure}$. The elastic portion of the EEPC contains the origin and has a slope equal to the elastic stiffness, k_e. The plastic portion of the EEPC is a horizontal line positioned so that the EEPC and actual load-drift curve areas are equal (i.e. areas A1 and A2 in Figure 5.3 are equal). Displacement at yield, Δ_{yield}, and load at yield, F_{yield}, were defined as the intersection of the elastic and plastic lines of the EEPC. By definition, F_{yield} must be greater than or equal to 80% of F_{max}. This definition of the EEPC was also used in the monotonic tests, and is similar to that used in the sequential phased displacement test developed by the Joint Technical Coordinating Committee on

Masonry Research (TCCMAR) for the United States - Japan Coordinated Earthquake Research Program and defined by Porter (1987).

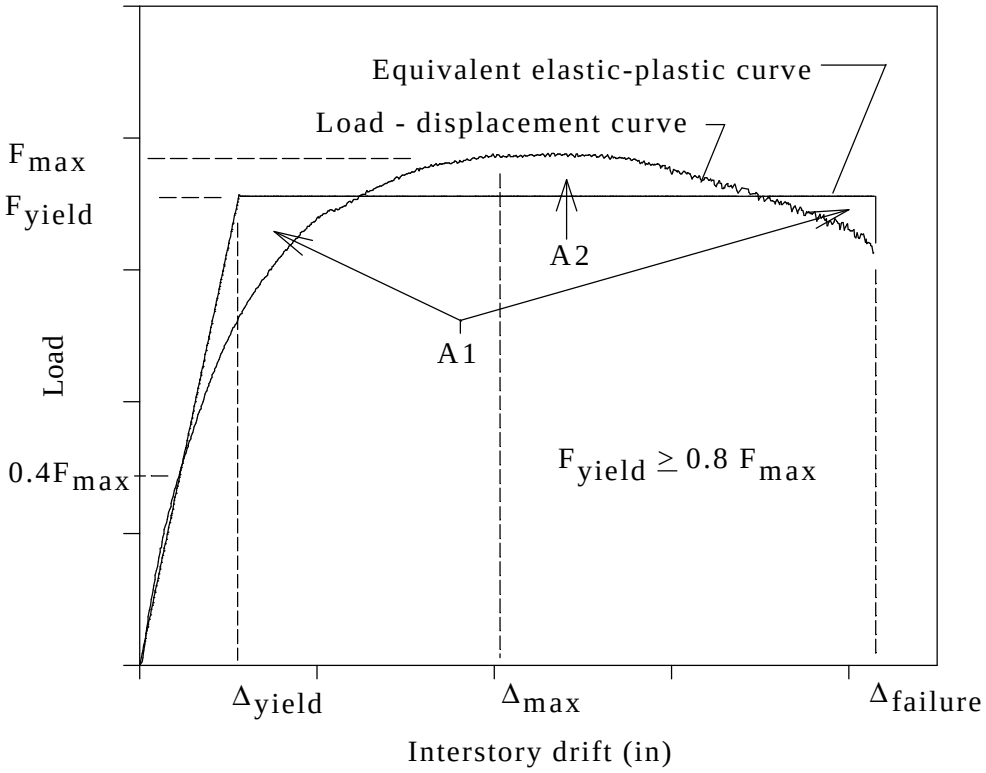

Figure 5. 3- Typical equivalent elastic-plastic curve

Load envelope curves consist of a positive and negative side, so two EEPC curves were created for each load envelope curve. The average of the positive and negative values obtained from the two EEPC curves were used to determine F_{yield}, Δ_{yield}, k_e, $F_{failure}$ and $\Delta_{failure}$.

From the EEPC, ductility is determined. Ductility is defined as:

$$D = \frac{\Delta_{failure}}{\Delta_{yield}} \tag{5.1}$$

where D is ductility, $\Delta_{failure}$ is drift at failure and Δ_{yield} is drift at yield.

5.3.3 Energy Definitions

A plot of load vs. interstory drift for one cycle of displacement, similar to the one shown in Figure 5. 4, was determined for the initial and stabilized cycle of each phase. Hysterisis loops associated with each initial and stabilized cycle for all phases experienced until failure were used for computing hysteretic energy, potential energy, and the equivalent viscous damping ratio (EVDR).

Hysteretic energy (HE) is the total area enclosed by the hysterisis curve for a given interstory drift and cycle. This is the amount of energy dissipated by the wall during one cycle.

Potential energy (PE) is one half the peak load times the maximum interstory drift for both the positive and negative displacements (i.e. the area inside triangles ABC and ADE in Figure 5. 4).

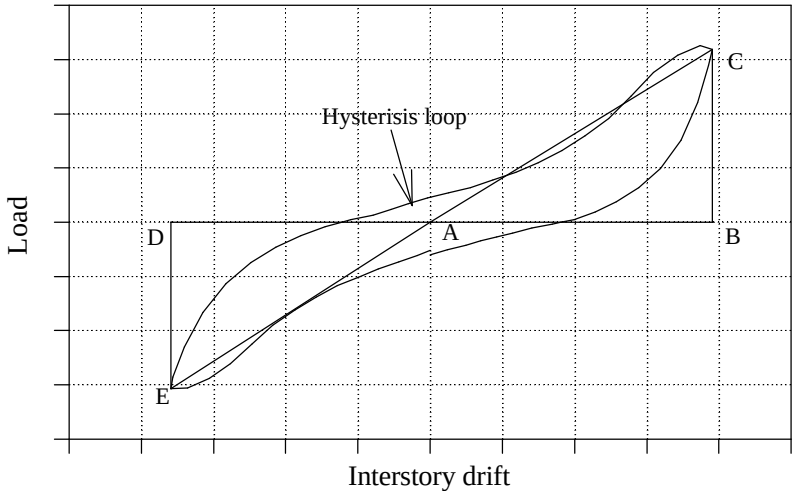

Figure 5. 4- Typical hysterisis loop for timber shear wall during SPD loading

Equivalent viscous damping ratio is defined as:

$$\mathrm{EVDR} = \frac{\mathrm{HE}}{2 \cdot \Pi \cdot \mathrm{PE}} \qquad (5.2)$$

EVDR is often used for comparing damping characteristics and for numerical modeling of the dynamic response of structures and is included here for future reference and use for numerical modeling.

5.4 SPD Test Results

5.4.1 Strength and Deflection

Figures 5.5 and 5.6 (and Appendices C-G) contain the initial cycle and stabilized cycle load-envelope curves for the five wall configurations tested. The general shape of the load-envelope curves are similar to the monotonic load-drift curves given in Figure 4.2, but several key differences exist. Peak load experienced during SPD loading was lower than monotonic capacity in all cases. Failure of the walls occurred at lower interstory drifts (under 2.5 in. (64 mm)) during SPD loaded shear wall tests than during monotonic shear wall tests. Figure 5.6 is similar to Figure 5.5, the main difference being stabilized load resistance, at a given interstory drift, is lower than

initial load resistance. At low magnitudes of load resistance, the shear walls were still behaving elastically and initial and stabilized load resistance were close to being equal.

It is noted in Figures 5.5 and 5.6 that slight differences in interstory drift exist among each wall configuration. The load cell displaced the top of the wall within 0.05 in. (1 mm) of the desired target before slip of the bottom sill was accounted for. Each wall experienced similar, but slightly different, slip of the bottom sill relative to the foundation, as measured by LVDT #3. As a result, each wall had slightly different interstory drifts in each phase of SPD loading. However, the differences are small when compared to displacement magnitude, and for practical purposes, the differences are insignificant.

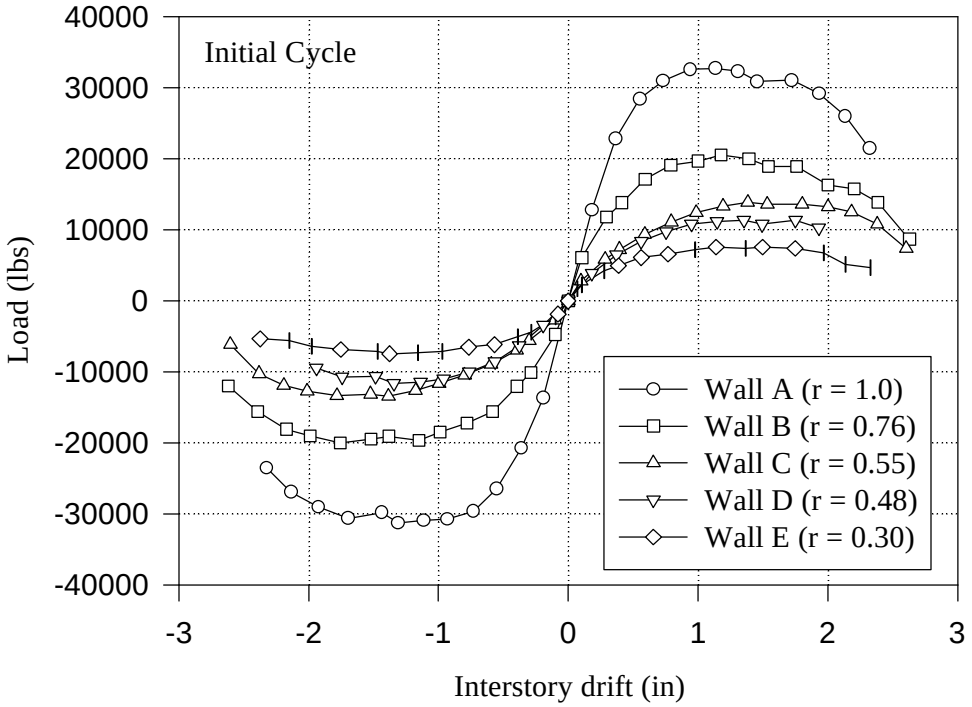

Figure 5. 5- Initial cycle load envelope curves for the five shear wall configurations examined

Tables 5.1 and 5.2 presents capacity data from the initial and stabilized cycle, respectively. Peak load resistance of the initial curve ranged from 7.5 kips (33.4 kN) to 32.0 kips (142.3 kN). Peak load resistance of the stabilized curve ranged from 6.6 kips (29.4 kN) to 27.5 kips (122.3 kN). These values correspond to a 77% and 76% change for initial cycle and stabilized cycle response respectively, when the fully sheathed wall capacities are used as the basis for comparison. In both cases, Wall E (r = 0.30) had the lowest capacity and Wall A (r = 1.0) had the highest capacity. The ratio of stabilized to initial capacity remained relatively constant, ranging from 86% to 88%. Stabilized capacity can be reasonably modeled as 87% of the initial cycle capacity, $F_{max,init}$.

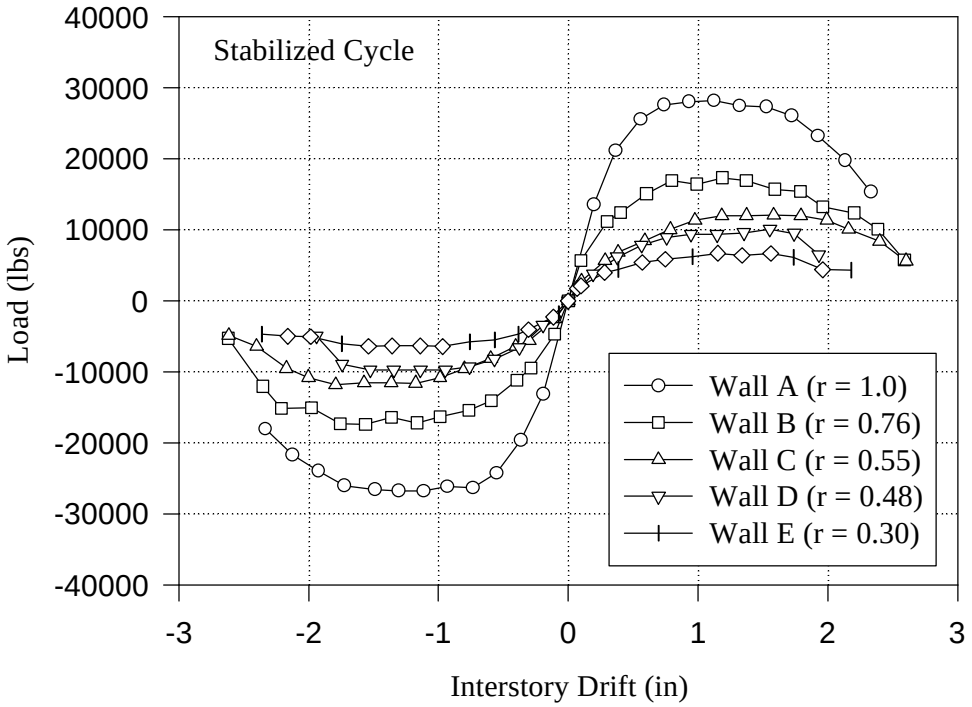

Figure 5. 6- Stabilized cycle load envelope curves for the five shear wall configurations examined

Table 5. 1: Initial cycle data of the five shear wall configurations examined

	Wall A	Wall B	Wall C	Wall D	Wall E
	r = 1.0	r = 0.76	r = 0.55	r = 0.48	r = 0.30
Initial					
F_{max} (kips)	32.0	20.3	13.6	11.5	7.5
Δ_{max} (in)	1.13	1.18	1.38	1.35	1.15
F_{yield} (kips)	29.9	18.4	12.4	10.4	6.8
Δ_{yield} (in)	0.43	0.47	0.62	0.58	0.37
$F_{failure}$ (kips)	29.1	17.6	12.2	9.8	6.6
$\Delta_{failure}$ (in)	1.93	2.00	2.19	1.94	1.97
k_e (kips/in)	69.7	40.0	19.9	18.1	18.2
F_{yield}/F_{max}	0.93	0.91	0.92	0.90	0.91
Ductility	4.5	4.3	3.5	3.3	5.3

Table 5. 2: Stabilized cycle data of the five shear wall configurations examined

	Wall A r = 1.0	Wall B r = 0.76	Wall C r = 0.55	Wall D r = 0.48	Wall E r = 0.30
Stabilized					
F_{max} (kips)	27.5	17.4	11.8	9.9	6.6
Δ_{max} (in)	1.12	1.19	1.37	1.55	1.15
F_{yield} (kips)	25.9	15.6	10.7	8.8	5.8
Δ_{yield} (in)	0.37	0.38	0.53	0.49	0.32
$F_{failure}$ (kips)	23.6	14.1	9.8	5.7	4.7
$\Delta_{failure}$ (in)	1.93	1.98	2.17	1.95	1.98
k_e (kips/in)	69.2	41.8	20.3	18.2	18.0
F_{yield}/F_{max}	0.94	0.90	0.91	0.89	0.88
Ductility	5.2	5.2	4.1	4.0	6.2

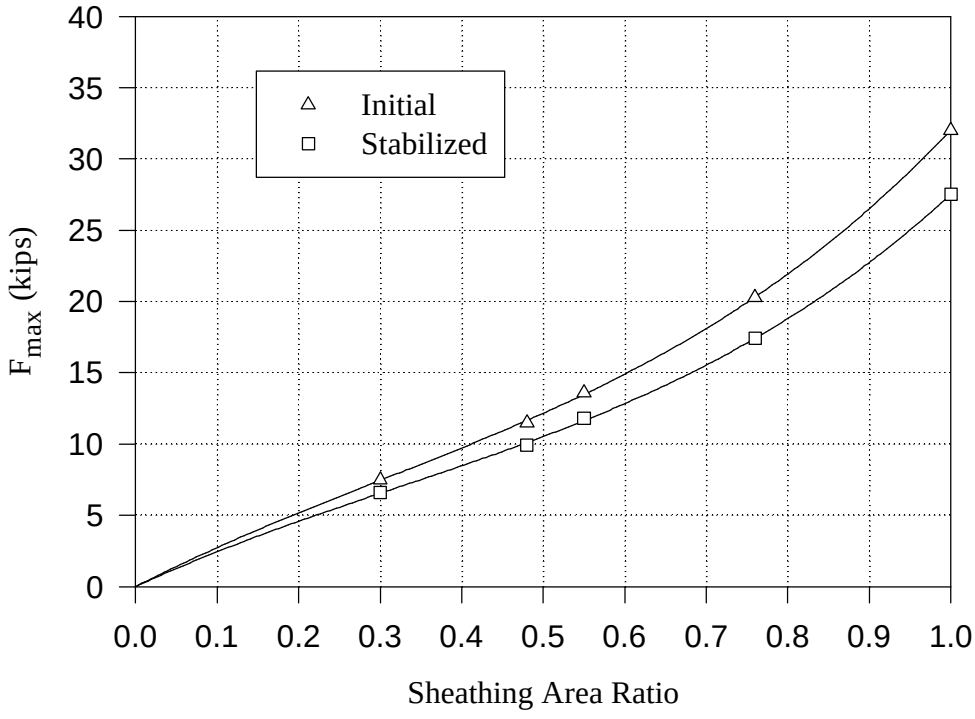

Figure 5. 7- Initial and stabilized cycle capacity of the five shear wall configurations examined plotted against sheathing area ratio

Figure 5. 7 plots initial and stabilized load capacity of each wall against sheathing area ratio, along with the best fit third order regressions. The best fit equation for initial capacity is:

$$F_{max} = 29.458 \cdot r - 23.090 \cdot r^2 + 25.633 \cdot r^3 \quad (5.3)$$

The best fit equation for stabilized capacity is:

$$F_{max} = 26.543 \cdot r - 22.932 \cdot r^2 + 23.889 \cdot r^3 \quad 5.4)$$

where F_{max} is capacity and r is sheathing area ratio.

Drift corresponding to capacity for the initial cycle, presented in Table 5.1, ranged from 1.12 in. (28 mm) for Wall A (r = 1.0) to 1.47 in. (37 mm) for Wall B (r = 0.76). As presented in Table 5.2, Δ_{max} for the stabilized cycle ranged from 1.02 in. (26 mm) for Wall E (r = 0.30) to 1.69 in. (43 mm) for Wall C (r = 0.55). Figure 5.8 shows Δ_{max} of the initial and stabilized cycles of the five wall configurations, as well as Δ_{yield} and $\Delta_{failure}$.

For the initial cycle, it is shown in Table 5. 1 that F_{yield} ranged from 6.8 kips (30.2 kN) for Wall E (r = 0.30) to 29.9 kips (133.0 kN) for Wall A (r = 1.0). For the stabilized cycle, it is shown in Table 5.2 that F_{yield} ranged from 5.8 kips (25.8 kN) for Wall E (r = 0.30) to 25.9 kips (115.2 kN) for Wall A (r = 1.0). For both the initial and stabilized cycles, F_{yield} was 89% to 93% of F_{max}. F_{yield} can reasonably be modeled as 90% of F_{max}.

Drift at yield, presented in Table 5.1 - 5.2 and illustrated in Figure 5.8, ranged from 0.37 in. (9 mm) to 0.62 in. (16 mm) for the initial cycle and 0.32 in. (8 mm) to 0.53 in. (13 mm) for the stabilized cycle. For both initial and stabilized cycles, Wall E had the lowest drift at yield and Wall C had the highest.

Load resistance at failure, presented in Table 5.1 and 5.2, ranged from 6.6 kips (29.4 kN) to 29.1 kips (129.4 kN) for the initial cycle and 4.7 kips (20.9 kN) to 23.6 kips (105.0 kN) for the stabilized cycle. As expected, Wall E had the lowest load resistance at failure and Wall A the highest. $F_{failure}$ ranged from 85% to 91% of F_{max} for the initial cycle.

Drift at failure, presented in Table 5.1 - 5. 2 and illustrated in Figure 5.8, ranged from 1.93 in. (49 mm) to 2.19 in. (56 mm) for the initial cycle and 1.93 in. (49 mm) to 2.17 in. (55 mm) for the stabilized cycle. For both initial and stabilized cycles, Wall A had the lowest drift at failure and Wall C had the highest.

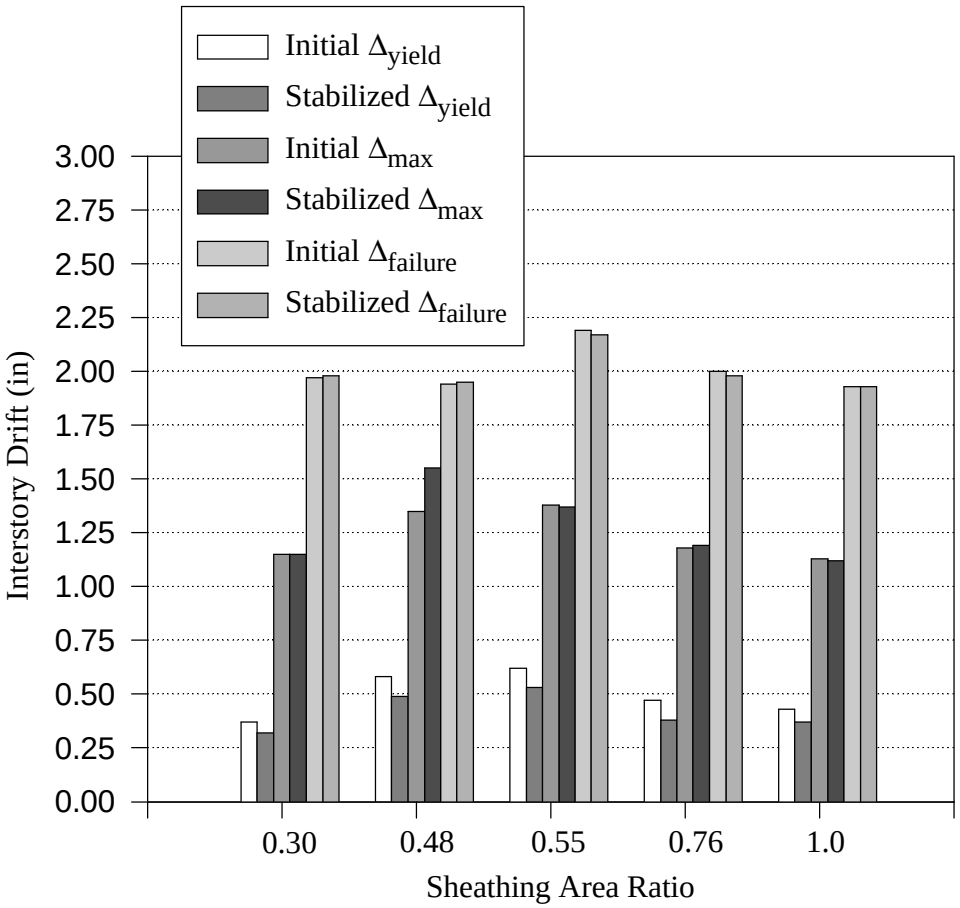

Figure 5. 8- Initial and stabilized drift corresponding to yield, capacity, and failure of the five shear wall configurations examined

5.4.2 Elastic Stiffness

Elastic stiffness for the initial cycle, as determined from the load-envelope curves and presented in Table 5.1, ranged from 18.1 kips/in (3200 kN/m) for Wall D (r = 0.48) to 69.7 kips/in (12200 kN/m) for Wall A (r = 1.0). Elastic stiffness for the stabilized cycle is presented in Table 5.2 and ranged from 18.0 kips/in (3150 kN/m) for Wall E (r = 0.30) to 69.2 kips/in (12100 kN/m) for Wall A (r = 1.0). Figure 5.9 plots elastic stiffness of the five wall configurations against sheathing area ratio.

It was expected that walls with more full height sheathing panels would have higher elastic stiffness than walls with less full height sheathing panels. This was not the case with Wall D, which had four fully sheathed panels, and Wall E, which had three fully sheathed panels. Cyclic elastic stiffness of the two walls were nearly identical. An examination of the wall configuration of Wall D (r = 0.48) shows that only one full height sheathing panel is adjacent to the load cell, followed by a 12 ft. (3.7 m) garage door opening. Wall E (r = 0.30) contains two full height sheathing panel adjacent to

the load cell followed by 28 ft. (8.5 m) with no sheathing. It is possible that the shear was not initially transferred the full length of the wall initially and the sheathing adjacent to the load cell resists higher shear than the sheathing farther from loading. This would explain the similar elastic stiffness of Walls C and D. It is noted that monotonic elastic stiffness of Wall D and E were not similar.

It was also expected that elastic stiffness would be higher than stabilized. At low interstory drifts, initial and stabilized load envelope curves are relatively equal. Elastic stiffness is taken at the interstory drift corresponding to 40% of capacity. Since stabilized capacity is always lower than initial capacity, the interstory drift corresponding to 40% of capacity is always lower for the stabilized cycle. At the interstory drift corresponding to 40% of capacity for the stabilized cycle, the load-envelope curve is linear. However, at the interstory drift corresponding to 40% of capacity for the initial cycle (which is higher than the stabilized cycle), the load-envelope curve is beginning to lose its elastic behavior. Due to differences in interstory drift where elastic stiffness is determined and the shapes of the load-envelope curves of the initial and stabilized cycle, stabilized elastic stiffness was higher than initial elastic stiffness for three shear walls with openings.

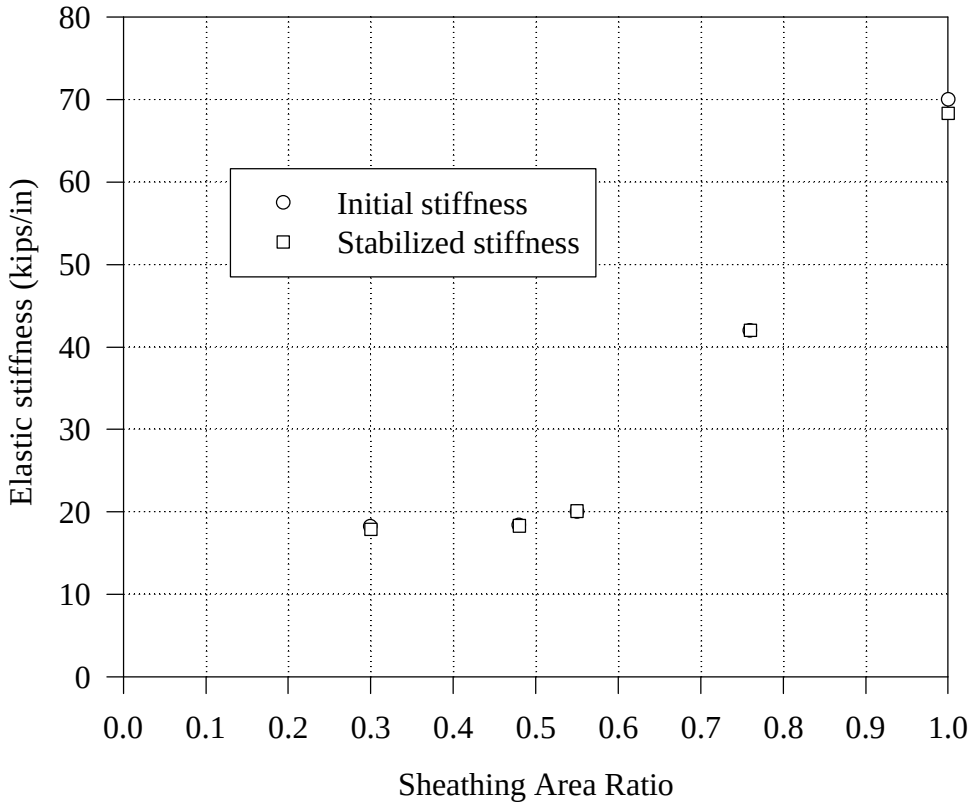

Figure 5. 9- Initial and stabilized elastic stiffness of the five shear wall configurations examined plotted against sheathing area ratio

Figure 5.10 examines the relationship between capacity and elastic stiffness for the five shear wall configurations examined. Figure 5.10 plots the shear strength ratio on the x- axis versus shear stiffness ratio on the y-axis. Shear strength ratio was defined as the ratio of capacity of a shear wall divided by the capacity of the fully sheathed wall. Similarly, shear stiffness ratio was defined as the ratio of elastic stiffness of a shear wall divided by the elastic stiffness of the fully sheathed shear wall. The general trend of the data is that there is slightly larger reduction in stiffness than for capacity for walls with openings when tested under cyclic displacements.

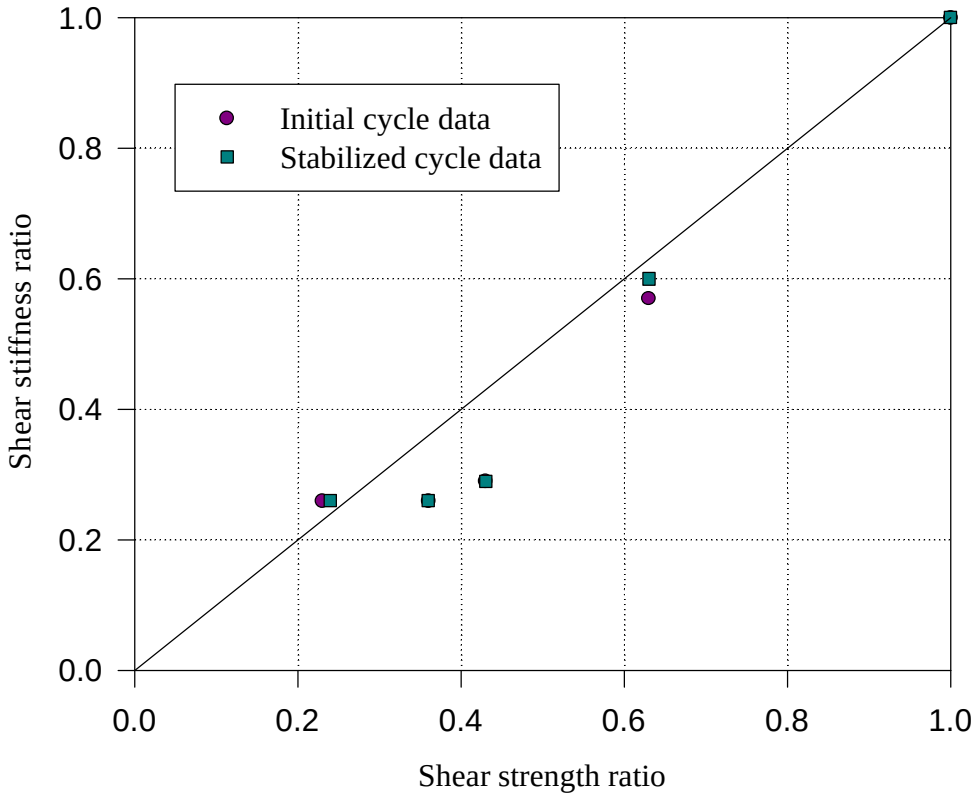

Figure 5. 10- Comparison of shear strength ratio and shear stiffness ratio of the five shear wall configuration examined under cyclic displacements

5.4.3 Ductility

As defined in Equation 5.1, ductility is the ratio of $\Delta_{failure}$ to Δ_{yield}. Deflection at yield is determined as load at yield divided by the elastic stiffness. As shown in the previous section, elastic stiffness was defined similarly for both the initial and stabilized envelope curves. Because F_{yield} is always higher for the initial cycle than the stabilizedcycle, Δ_{yield} also will always be higher for the initial cycle. Because drift at failure is always the same for both initial and stabilized cycles and initial Δ_{yield} is

higher than stabilized Δ_{yield}, it is expected that the initial cycle ductility is lower than the stabilized cycle ductility.

Tables 5.1 and 5.2 provide drift data at yield and failure for initial and stabilized cycles. Ductility, presented in Tables 5.1 and 5.2 and illustrated in Figure 5.11, ranged from 3.3 to 5.3 for the initial cycle and ranged from 4.0 to 6.2 for the stabilized cycle. As expected, initial ductility was lower than stabilized ductility. The ratio of initial to stabilized ductility fell in the range of 83% to 87% for the five wall configurations. No correlation was found between ductility and sheathing area ratio.

While providing an important indication of performance, ductility must be viewed in relation to stiffness, yield resistance, and capacity to provide an overall evaluation of performance.

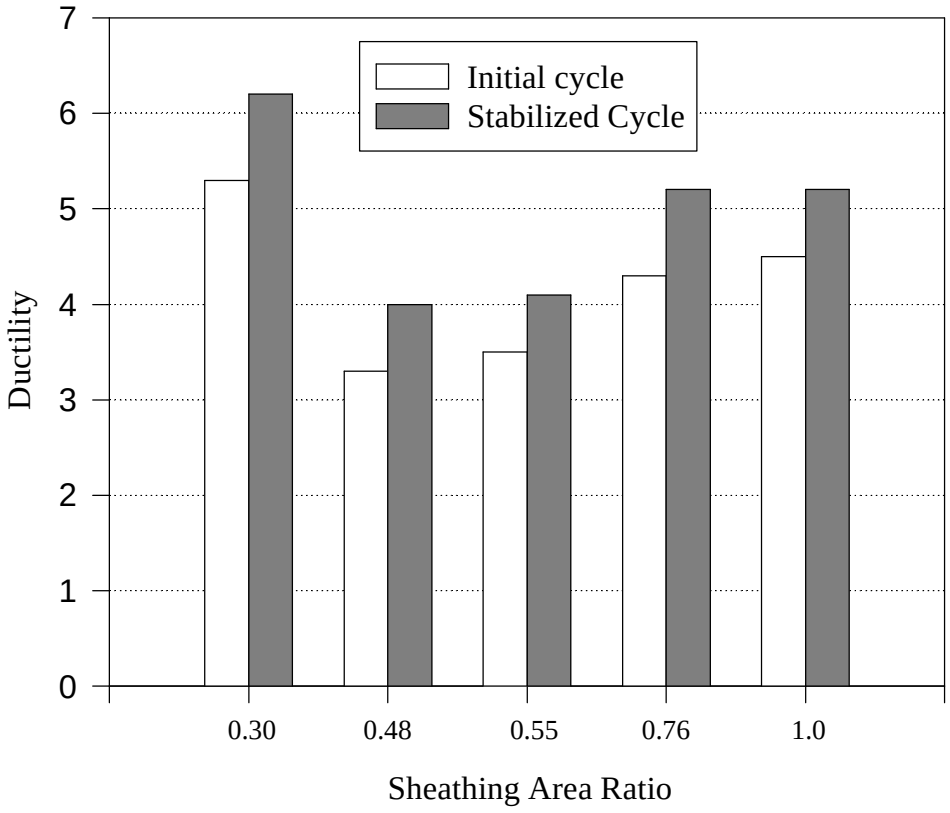

Figure 5. 11- Initial and stabilized ductility ratios of the five shear wall configurations examined

5.4.4 Cyclic Stiffness and Energy

Appendices C - G presents the hysteresis loops for the initial and stabilized cycles of the five wall configurations examined in this thesis. Appendix B contains tabulated cyclic stiffness energy data discussed in this section for each phase of SPD loading experienced until failure.

5.4.4.1 Cyclic Stiffness

Stiffness of a wall is primarily a function of the ability of the sheathing nails to distribute load. More sheathing nails results in higher stiffness. Since rate of loading and the number of repetitive cycles effect nail performance, stiffness must be viewed with these three variables in mind. While the rate of loading was such that the inertial effects of the wall and test fixture were not effecting the test, the number of cycles did. Many of the sheathing nails failed in fatigue near the end of the test, which is not a common failure mode observed in the field. Therefore, these results must be viewed with the uncommon fatigue effects considered. Cyclic stiffness, k_c, was used to help define the behavior of shear walls during cyclic loading and was determined as the average of the slopes of lines AC and AE in Figure 5.4.

Cyclic stiffness of the initial and stabilized cycles for each phase was plotted as a function of interstory drift in Figures 5.12 - 5.13, respectively. As expected, as the wall experienced higher drifts, cyclic stiffness decreased. The rate of stiffness degradation is based on the type and number of connections used, and in this thesis, the number of 8d (0.131 in. (3 mm) diameter and 2.5 in. (64 mm) length) plywood sheathing nails primarily controlled stiffness degradation. As the walls experienced increased loads at increased interstory drifts, sheathing nails were progressively damaged and friction between the nails and wood members decreased, causing cyclic stiffness to decrease. Due to damage between the initial cycle of displacement and the stabilized cycle of displacement in a given phase, initial stiffness is always higher than stabilized stiffness. As previously stated in Section 5.4.1, differences in sensor readings of the top and bottom wall displacements result in slight differences in interstory drift. Tables B1 - B5 in Appendix B present initial and stabilized cyclic stiffness and interstory drift for each phase of SPD loading.

5.4.4.2 Hysteretic energy

Figures 5.14 and 5.15 present the initial cyclic and stabilized cyclic hysteretic energy data as a function of interstory drift and Tables B1 - B5 in Appendix B present hysteretic energy for each phase of SPD loading. Hysteretic energy increased as the interstory drift increased until near failure of the wall. As shown in Table 5.3, peak hysteretic energy experienced between 0 in. drift and $\Delta_{failure}$ ranged from 10.6 kips-in (1.20 kN-m) for Wall E (r = 0.30) to 41.4 kips-in (4.67 kN-m) for Wall A (r = 1.0) during the initial cycle and 8.6 kips-in (0.97 kN-m) for Wall E (r = 0.30) to 32.4 kips-in (3.66 kN-m) for Wall A (r = 1.0) during the stabilized cycle. Drift corresponding to peak hysteretic energy is also given in Table 5.3. Peak hysteretic energy was experienced at failure or during the phase prior to failure. Both Figures 5.14 and 5.15 are similar, but initial hysteretic energy is higher than stabilized hysteretic energy at each interstory drift.

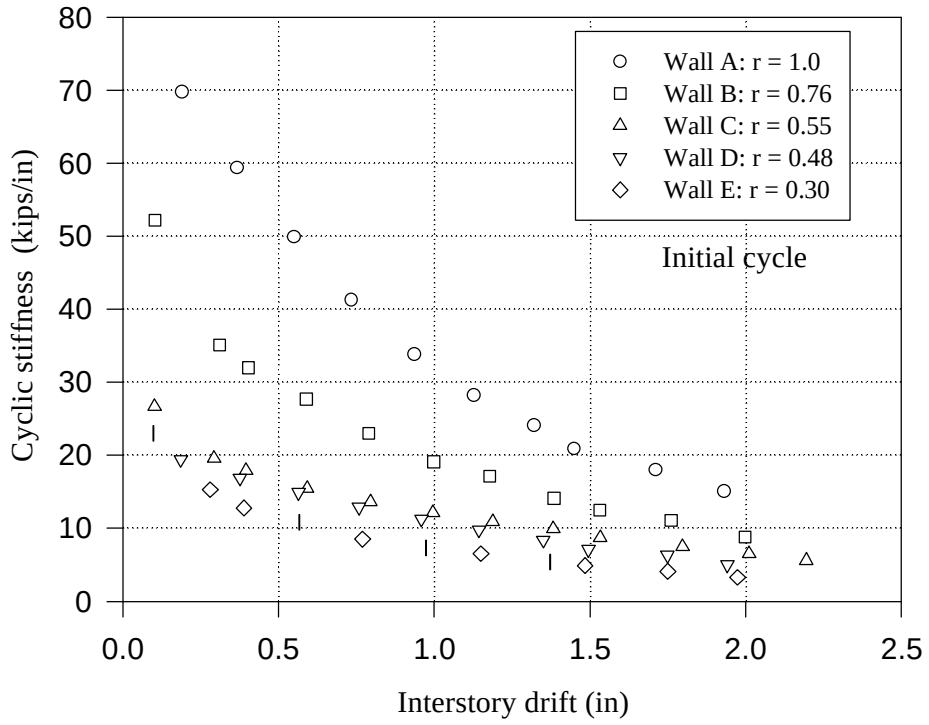

Figure 5. 12- Initial cyclic stiffness of the five shear wall configurations examined plotted against interstory drift

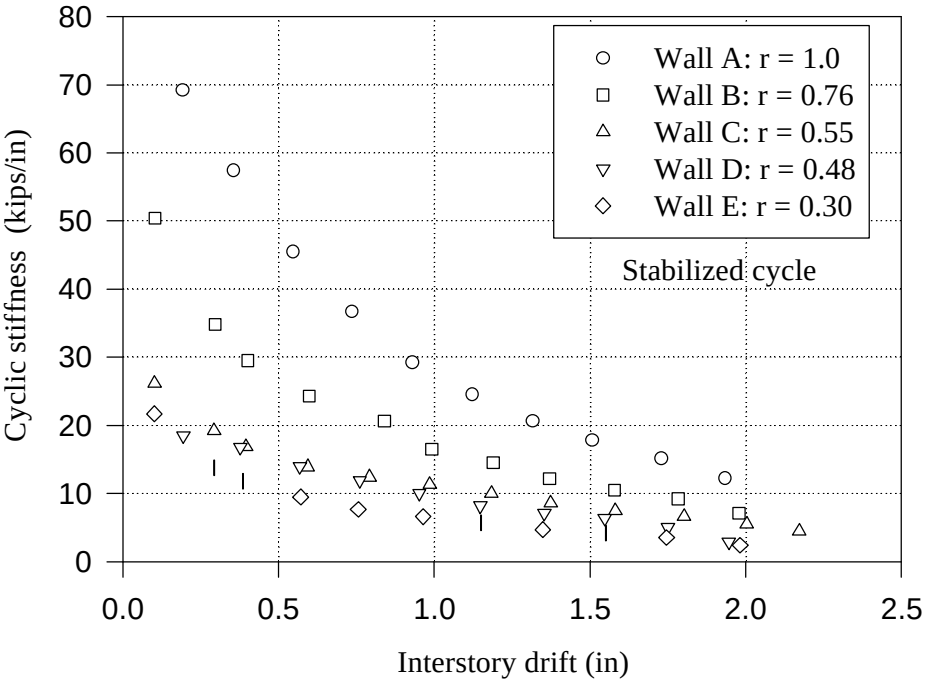

Figure 5. 13- Stabilized cyclic stiffness of the five shear wall configurations examined plotted against interstory drift

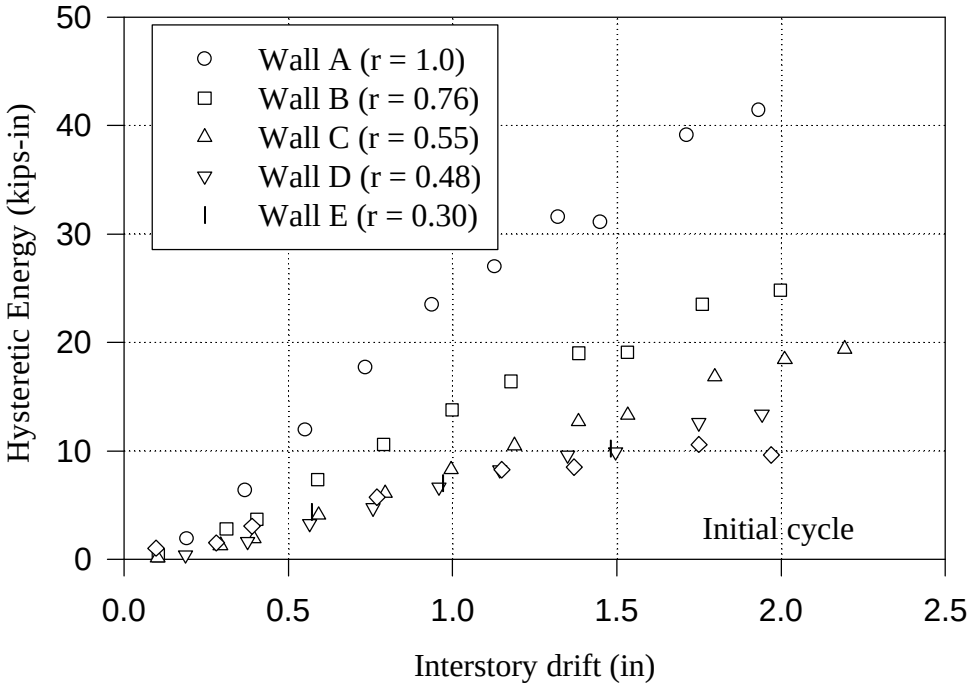

Figure 5. 14- Initial hysteretic energy of the five shear wall configurations examined plotted against interstory drift

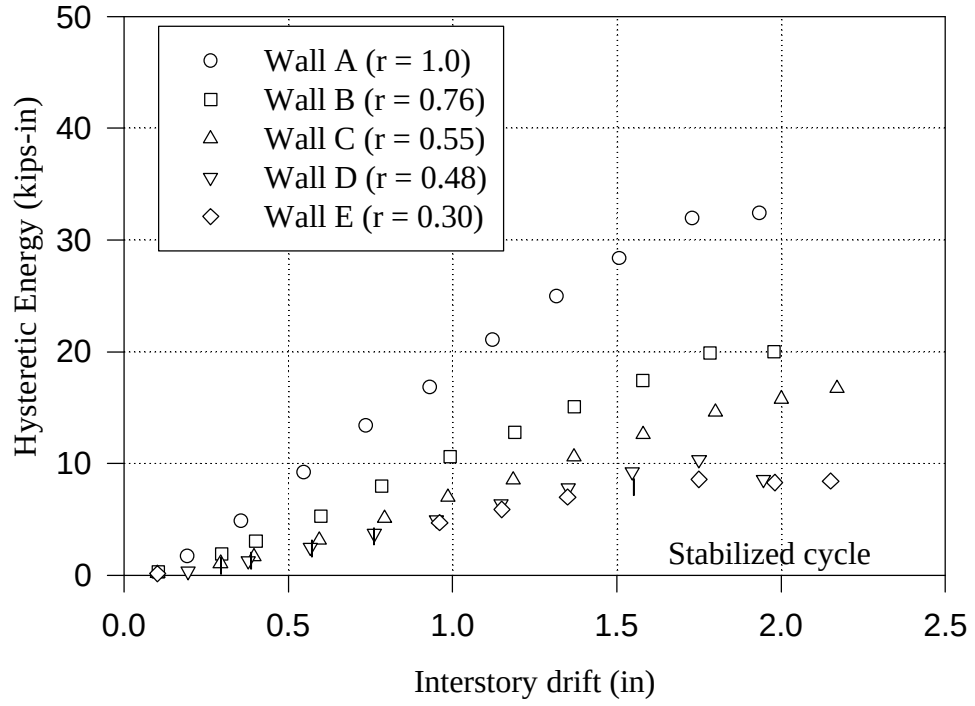

Figure 5. 15 - Stabilized hysteretic energy of the five shear wall configurations examined plotted against interstory drift

Table 5. 3: Initial and stabilized peak hysteretic and potential energy of the five shear wall configurations examined

	Wall A	Wall B	Wall C	Wall D	Wall E
	r = 1.0	r = 0.76	r = 0.55	r = 0.48	r = 0.30
max. H.E., initial (kips-in) @ drift (in)	41.4 (1.93)	24.8 (2.00)	19.4 (2.19)	13.4 (1.94)	10.6 (1.75)
max H.E., stab. (kips-in) @ drift (in)	32.4 (1.93)	20.0 (1.98)	16.7 (2.17)	10.4 (1.75)	8.6 (1.55)
max P.E., initial (kips-in) @ drift (in)	56.3 (1.93)	35.6 (2.00)	26.8 (2.19)	19.2 (1.75)	12.9 (1.75)
max P.E., stab. (kips-in) @ drift (in)	45.6 (1.93)	29.2 (1.78)	22.1 (2.00)	16.0 (1.75)	10.6 (1.55)

It becomes obvious that the primary source of hysteretic energy dissipation for wood shear walls is the yielding of the sheathing nails and friction between the sheathing and framing. Wall A has the highest value for hysteretic energy dissipated, and it also has the most sheathing and nails. Wall E has the minimum values for hysteretic damping and the least amount of sheathing and nails. It is noted that a drop in initial cycle hysteretic energy occurred near an interstory drift of 1.5 in. (38 mm) for both Wall A and B. This drop indicates a failure of a panel at the phase of SPD loading. Load was re-distributed to the other panels, enabling the wall to continue resisting load for two more phases until failure at a peak displacement of 2.0 in. (51 mm).

5.4.4.3 Potential energy

As defined in Section 5.3.3, potential energy is area under the triangle given by ABC and ADE in Figure 5.4. Figures 5.16 and 5.17 present the initial cyclic and stabilized cyclic potential energy data as a function of interstory drift and Tables B1 - B5 in Appendix B present potential energy data for each phase of SPD loading. Potential energy follows a similar trend as hysteretic energy, but, due to the typical pinched hysteresis loops of light-frame shear walls, potential energy is higher than hysteretic energy for a given cycle. Maximum potential energy experienced between 0 in. drift and $\Delta_{failure}$ for both the initial and stabilized cycle are given in Table 5.4, as well as corresponding drift. For the initial cycle, peak potential energy ranged from 12.9 kips-in (1.46 kN*m) for Wall E (r = 0.30) to 56.3 kips-in (6.36 kN*m) for Wall A (r = 1.0). Peak potential energy for the stabilized cycle ranged from 10.6 kips-in (1.20 kN*m) for Wall E (r = 0.30) to 45.6 kips-in (5.15 kN*m) for Wall A (r = 1.0).

As with hysteretic energy, potential energy is directly related to the amount of sheathing and number of sheathing nails present. This is because the framing supports vertical loads while the sheathing provides the racking resistance for the assembly.

5.4.4.4 Equivalent viscous damping ratio

The equivalent viscous damping ratio (EVDR) for the initial and stabilized cycles at or near Δ_{yield}, Δ_{max}, and $\Delta_{failure}$ are presented in Table 5.4 and illustrated in Figures 5.18 and 5.19. At yield, EVDR ranged from 0.111 to 0.127 for the initial cycle and 0.088 to 0.118 for the stabilized cycle. At capacity, EVDR ranged from 0.099 to 0.131 for the initial cycle and 0.095 to 0.123 for the stabilized cycle. At failure, EVDR ranged from 0.108 to 0.133 for the initial cycle and 0.112 to 0.151 for the stabilized cycle. At yield and capacity, initial EVDR tended to be higher than stabilized EVDR. At failure, stabilized EVDR was generally higher.

Based on this limited data, initial EVDR of similar shear walls can reasonably be modeled as 0.11 and stabilized EVDR can be reasonably be modeled between 0.10 and 0.105 prior to failure.

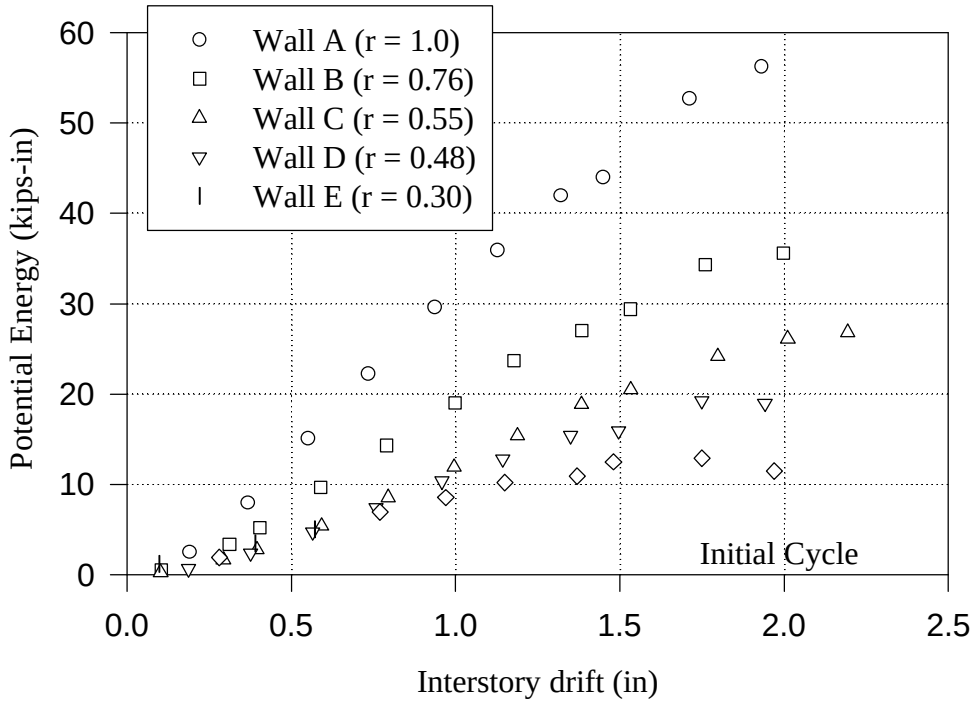

Figure 5. 16 - Initial potential energy of the five shear wall configurations examined plotted against interstory drift

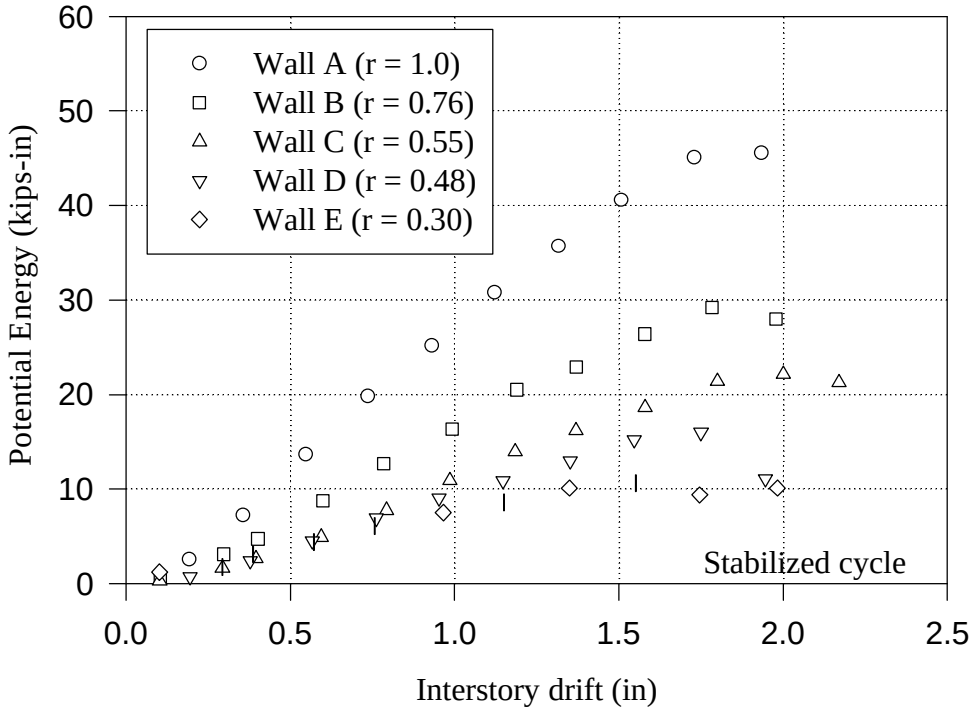

Figure 5. 17- Stabilized potential energy of the five shear wall configurations examined plotted against interstory drift

Table 5. 4: Initial and stabilized equivalent viscous damping ratio (EVDR) at or near Δ_{yield}, Δ_{max}, and $\Delta_{failure}$ for the five shear wall configurations examined

	Wall A	Wall B	Wall C	Wall D	Wall E
	r = 1.0	r = 0.76	r = 0.55	r = 0.48	r = 0.30
Initial cycle:					
EVDR @ or near:					
Δ_{yield}	0.127	0.111	0.121	0.111	0.125
Δ_{max}	0.120	0.113	0.107	0.099	0.131
$\Delta_{failure}$	0.113	0.108	0.129	0.112	0.133
Stabilized cycle:					
EVDR @ or near:					
Δ_{yield}	0.106	0.102	0.102	0.088	0.118
Δ_{max}	0.108	0.106	0.108	0.095	0.123
$\Delta_{failure}$	0.112	0.127	0.151	0.129	0.141

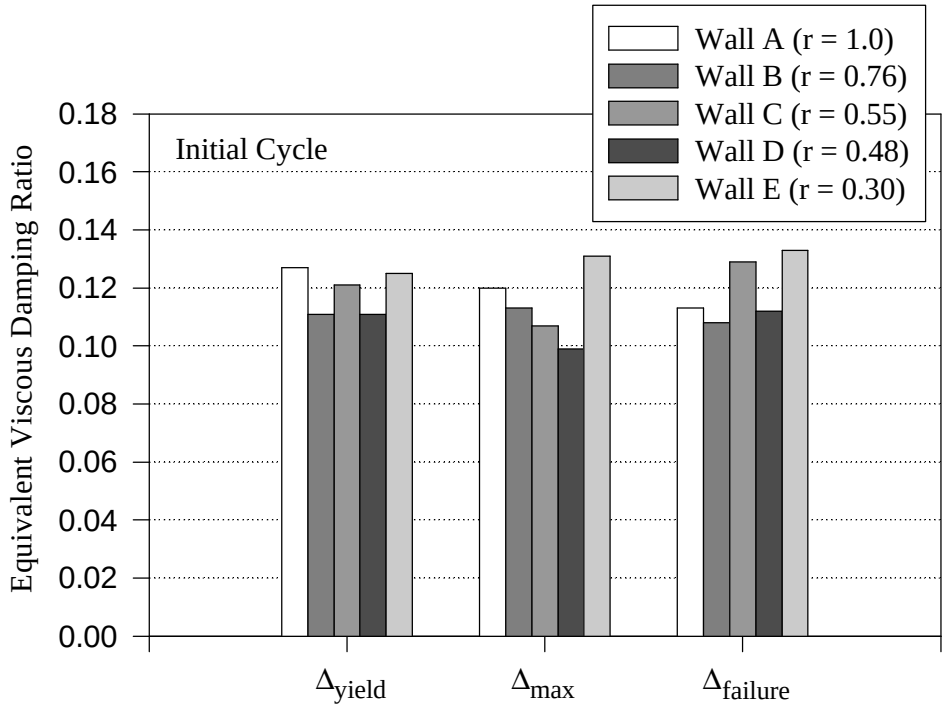

Figure 5. 18- Initial cycle equivalent viscous damping ratios (EVDR) of the five shear wall configurations examined at Δ_{yield}, Δ_{max}, and $\Delta_{failure}$

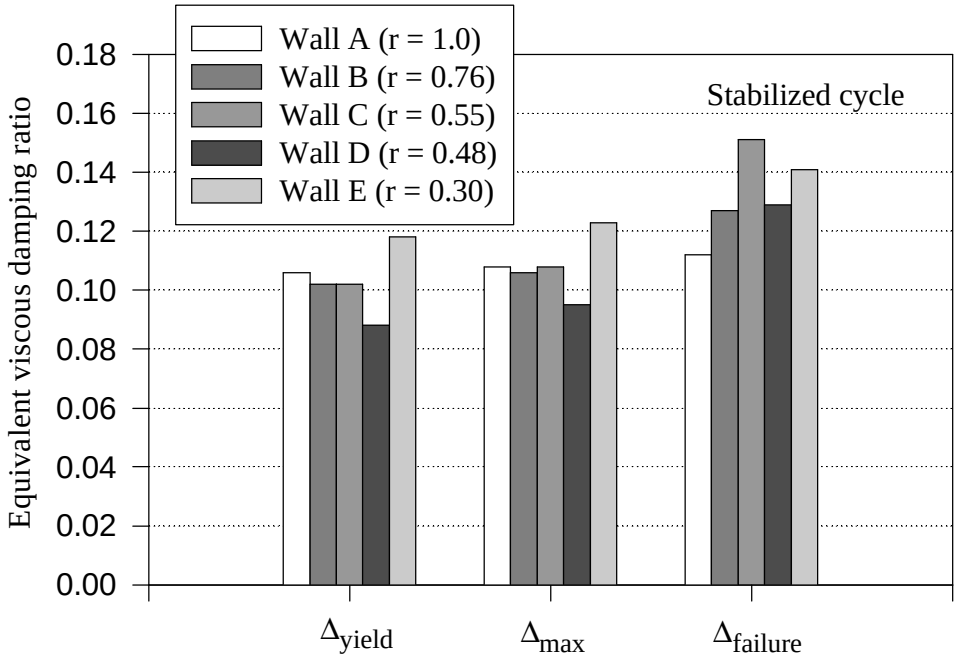

Figure 5. 19- Stabilized cycle equivalent viscous damping ratios (EVDR) of the five shear wall configurations examined at Δ_{yield}, Δ_{max}, and $\Delta_{failure}$

5.4.5 Wall Behavior

As discussed in Section 3.5, six external LVDT's were placed on the shear walls to monitor movement of the end studs relative to the bottom plate, slip of the tie-down anchors relative to the end studs and displacement of the top and bottom plates.

5.4.5.1 End Studs

As expected, SPD loading caused cyclical movement of the end studs relative to the bottom plate. The distance traveled by the end studs between peak positive and negative interstory drifts (i.e. between point A to B in Figure 5.1), recorded during the initial cycle at Δ_{max} and $\Delta_{failure}$, are given in Table 5.5. The reported movement of the end studs was determined at 1.5 in. (38 mm) from the end of the wall (i.e. at the center of the double end studs) near the bottom plate. This value is corrected from the actual LVDT value to account for the geometry effects of the fixture holding the LVDT.

Figure 5.20 plots typical movement of the end stud motion relative to the bottom plate during SPD loading against time. From Table 5.5, left end stud movement at Δ_{max} ranged from 0.098 in. (2.5 mm) to 0.179 in. (4.5 mm) and right end stud movement at Δ_{max} ranged from 0.097 in. (2.5 mm) to 0.141 in. (3.6 mm). At failure, left end movement ranged from 0.187 in. (4.7 mm) to 0.211 in. (5.4 mm) and right end stud movement ranged from 0.136 in. (3.5 mm) to 0.231 in. (5.9 mm). The tie-down anchors are responsible for keeping movement of the end studs to a minimum.

Table 5. 5: Initial cycle end stud displacement between positive and negative peak drifts at Δ_{max} and $\Delta_{failure}$ for the five shear wall configurations examined

	Wall A r = 1.0	Wall B r = 0.76	Wall C r = 0.55	Wall D r = 0.48	Wall E r = 0.30
Left end stud (LVDT #1) at Δ_{max} (in)	0.142	0.120	0.179	0.100	0.098
Right end stud (LVDT #2) at Δ_{max} (in)	0.141	0.097	0.103	0.140	0.141
Left end stud (LVDT #1) at $\Delta_{failure}$ (in)	0.211	0.187	0.211	*	0.199
Right end stud (LVDT #2) at $\Delta_{failure}$ (in)	0.203	0.167	0.136	0.197	0.231

*Sensor was moved during testing

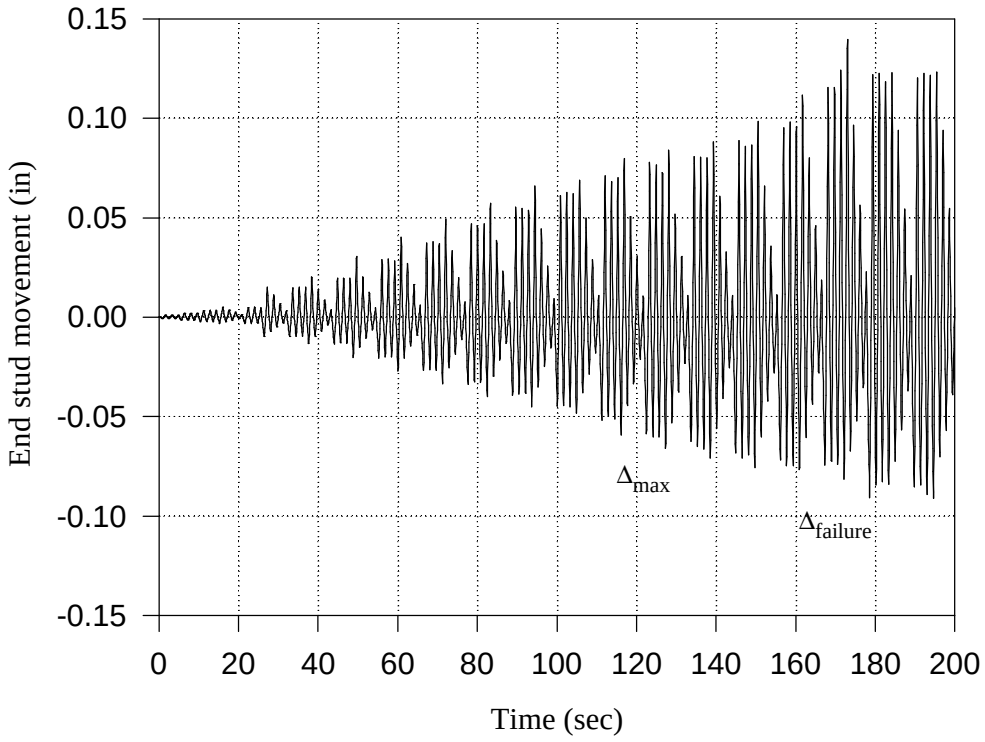

Figure 5. 20- Typical end stud movement recorded during SPD loading

5.4.5.2 Tie-down Anchors

Failures in past earthquakes have been attributed to slip or separation of the tie-down anchor from the double end studs to which the devices were attached. For purposes of monitoring slip between the anchor and the end stud, a LVDT was placed on each metal tie-down anchor. Slip relative to the stud for anchors, recorded near peak load, was found to be negligible for all wall configurations tested using SPD loading. According to Table 5.6, the distance traveled by the end stud relative to the tie-down between peak positive and negative drifts (i.e. between points A and B in Figure 5.1), recorded during the initial cycle at capacity ranged from 0.009 in. (0.2 mm) to 0.031 in. (0.8 mm) for LVDT #4 and 0.000 in. (0 mm) to 0.081 in. (0.2 mm) for LVDT #5.

Table 5. 6: Initial cycle slip of tie-down anchors relative to end studs for Walls A, B, C, and E

	Wall A	Wall B	Wall C	Wall E
	r = 1.0	r = 0.76	r = 0.55	r = 0.30
Slip of left tie-down (LVDT #4) (in)	0.009	0.031	0.011	0.027
Slip of right tie-down (LVDT #5) (in)	0.000	0.081	0.002	0.035

5.4.5.3 Failure Modes

Similar to the monotonic tests, fully sheathed plywood panels performed in a racking manner while plywood sheathing above and below openings did not rack. Gypsum panels underwent rigid body motion about their centers. Predominant failure of the sheathing was due to failure of the nails. Drywall nails simply tore a path through the relatively weak gypsum wallboard, due to the cyclic motion of the wall. The 8d (0.131 in. (3.3 mm) diameter and 2.5 in. (63.5 mm) length) plywood nails experienced partial withdrawal from the framing and fatigue. Nailing on the perimeter of plywood panels, especially near corners, experienced more fatigue than field nailing. Once corner nailing fatigue occurred the nails lost capacity to transfer shear, and the remaining nails had to resist the additional load previously carried by the corner nails. This occurred until the remaining nails could no longer transfer shear. Some tear through the edge of plywood panels was observed, but the amount was significantly less than in monotonic tests. The predominant mode of failure was fatigue of plywood nailing.

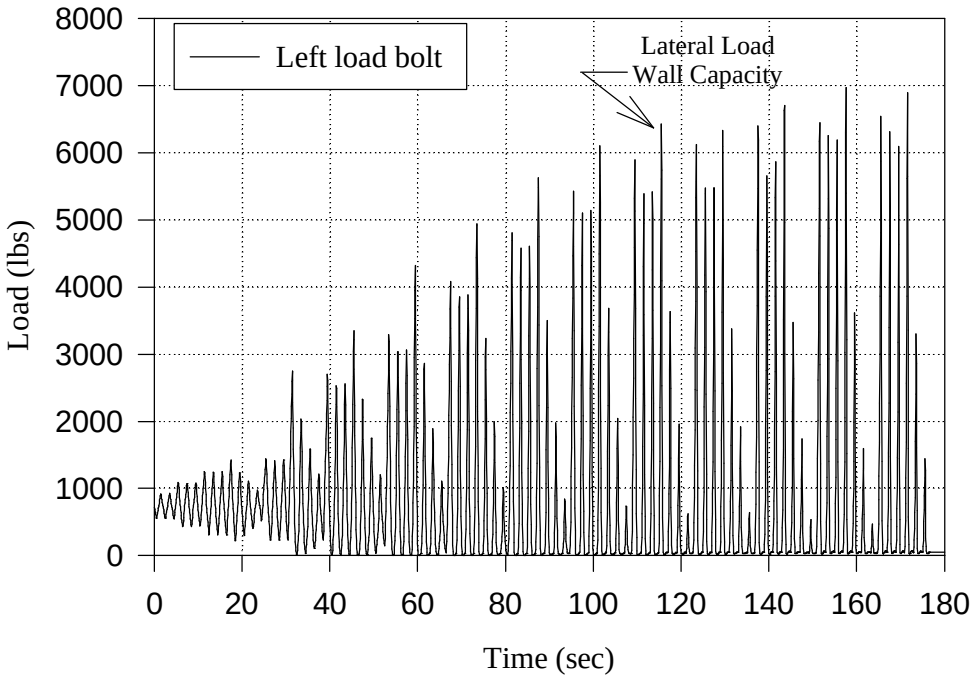

Figure 5. 21- Tension load resisted by left load bolt of Wall C (r = 0.55) plotted as a function of time

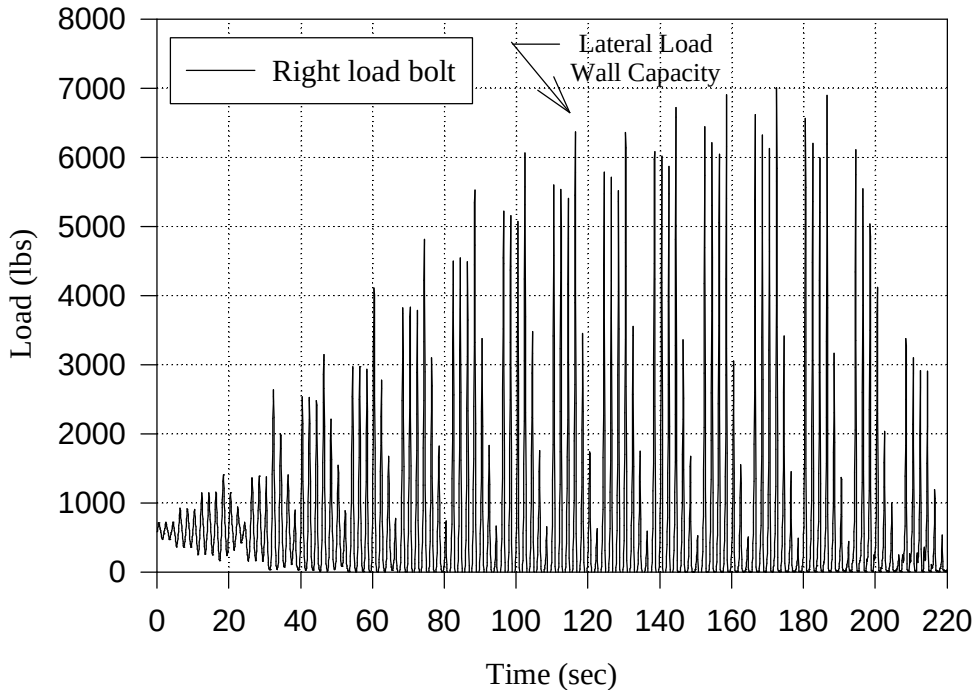

Figure 5. 22- Tension load resisted by right load bolt of Wall C (r = 0.55) plotted as a function of time

5.4.5.4 Tension Tie-down Anchor Bolts

Tension load bolts were used for SPD loading of Wall C (r = 0.55). Figures 5.21 and 5.22 plot load resisted by the left and right load bolts, respectively, during SPD loading All tie-down anchor bolts were pre-tensioned by hand when installed. The amount of pre-tensioning is indicated by the load magnitude carried by the load bolts at time zero in Figures 5.21 and 5.22.

Correlation of racking load resisted by the shear wall to load resisted by the bolt for each cycle in the test was determined. At initial cycle capacity, a racking load of 13,600 lbs (60.5 kN) was resisted by the wall, the left load bolt resisted 6420 lbs (28.6 kN) and the right load bolt resisted 6390 lbs (28.4 kN).

The best estimate of panel shear capacity for end panels are based on results from the fully sheathed wall. From Wall A, the unit shear capacity equals 32.0 kips / 40 ft., or 800 plf (11700 N/m). Calculation of the tie-down force would then be equal to 800 plf times the wall height of 8 ft., or 6,400 lbs (28.5 kN). At capacity, current design procedures for this wall specimen were in good agreement with the actual resistance of the anchor bolts.

Due to the tie-down anchors, the end panels have higher stiffness than panels without tie-down anchors. Greater uplift of the studs from the bottom sill was observed in the two interior full height panels compared to panels with anchorage. The panel without

anchorage closest to loading was the first to completely separate from the bottom plate. Tie-down anchorage would have allowed these panels to resist lateral loading at higher interstory drifts and is recommended in areas prone to seismic events.

It is noted that the design value of 6400 lbs (30.2 kN) to resist the overturning moment is based on the actual unit shear. Based on the unit shear determined using the 1994 UBC, the uplift design force would be 6140 lbs (27.3 kN).

5.5 Prediction of Capacity

This section presents two methods of prediction of shear walls with openings that only have tie-down anchorage at the ends of the wall. Both prediction methods rely upon the known capacity of the fully sheathed wall with identical materials and dimension. Since the actual capacity of the fully sheathed wall is not known in design situations, the capacity determined from current design procedures can be used in the two prediction methods. For this reason, this section first discusses the capacity using current design procedures and then examines the two prediction methods.

5.5.1 Current Code Design

Capacity determined from current design methodology for shear walls is the same regardless of hurricane or earthquake loading. Seismic forces are modified to equivalent static forces that are added to the lateral load that must be resisted by the shear wall. To determine the capacity of the shear walls examined in this thesis, the following equation is used:

$$V_{wall} = (V_{ply,\,ult}) \cdot \text{Length of full height wall segments} \qquad (5.5)$$

where V_{wall} is the ultimate capacity of the shear wall and $V_{ply,ult}$ is the ultimate shear for plywood sheathing.

Allowable shear for 15/32 in. (12 mm) structural I plywood with 8d nails at 6 in. (152 mm) perimeter spacing is 280 plf (4100 N/m) (UBC 1994). A factor of 0.82 must be applied to this value to account for the lower specific gravity of the spruce-pine-fir framing used in this experimental study. From APA report PRP-108, shear wall criteria is based on a minimum load factor of 2.8.

For the fully sheathed shear wall examined in this investigation, Equation 5.5 becomes:

$$V_{wall} = \left[280 \text{ plf} \cdot (2.8) \cdot (0.82)\right] \cdot 40'$$
$$= 25{,}700 \text{ lbs} \,(114 \text{ kN})$$

The capacity of the wall corresponds to a unit shear of 640 plf (9400 N/m).

Current design methodology of shear walls with openings only considers full height wall segments to resist lateral load. Proper anchorage must be designed by the engineer to ensure that each shear wall panel can transfer shear adequately. The walls

examined in this thesis had tie-down anchors at the ends of the wall only. Walls that contained openings contained two shear wall panels with only one tie-down anchor each, and the other shear wall panels (if any) did not contain tie-down anchors at all. Wall B (r = 0.76) consisted of three wall segments, Wall C (r = 0.55) and Wall D (r = 0.48) consisted of four wall segments and Wall E consisted of two.

Actual and design capacities, as well as the actual load factors (actual capacity/ allowable capacity), are presented in Table 5.7. For the shear walls examined in this thesis, current design methodology with conservative load factors recognizes full shear wall panels to carry 640 lbs/ft (9400 N/m). For 3 out of the 4 walls containing openings, initial shear resistance was greater than 640 lbs/ft (9400 N/m), indicating conservative design. The initial cycle unit shear of Wall E (r = 0.30) was unconservative by 3%. For the stabilized cycle unit shear at capacity, only Walls A and C had actual unit shears greater than the design unit shear. Walls B and D had 97% of the strength of thedesign unit shear. Wall E had 86% of the strength of the design unit shear, indicating that the construction technique of only having full height sheathing members at the ends of the wall should not be used in seismic zones.

Actual load factors, given in Table 5.7, ranged from 2.7 to 3.7 for the initial cycle and 2.4 to 3.2 for the stabilized cycle. Load factors tend to decrease as the area of openings increases, with the exception of Wall C (which contained the highest load factor). Wall C had the largest area of sheathing panels above and/or below openings relative to fully sheathed panels. Sheathing above and/or below openings is not accounted for to resist shear in design, but the high load factor of Wall C indicates that this sheathing does help resist lateral load.

Table 5. 7: Comparison of initial and stabilized capacity of the five shear wall configurations examined with ultimate design capacity

	Wall A r = 1.0	Wall B r = 0.76	Wall C r = 0.55	Wall D r = 0.48	Wall E r = 0.30
Design Capacity (kips/klf)	25.6/0.64	17.9/0.64	10.2/0.64	10.2/0.64	7.7/0.64
Initial Capacity (kips/klf)	32.0/0.80	20.3/0.73	13.6/0.85	11.5/0.72	7.5/0.63
Actual/ Design	1.25	1.13	1.33	1.13	0.97
Actual Load Factor	3.5	3.2	3.7	3.1	2.7
Stabilized Capacity (kips/klf)	27.5/0.69	17.4/0.62	11.8/0.74	9.9/0.62	6.6/0.55
Actual/ Design	1.07	0.97	1.16	0.97	0.86
Actual Load Factor	3.0	2.7	3.2	2.7	2.4

5.5.2 Application of Sugiyama's Method

Shear load ratios were determined as load resisted by a shear wall with openings divided by the load resisted by a shear wall of the same dimensions without openings. Sugiyama developed empirical equations to predict the shear load ratios of shear walls loaded monotonically. Sugiyama did not perform cyclic tests, and therefore, was unable to verify if his shear load ratios were valid for cyclic loading.

Shear load ratio, f, at an apparent shear deformation angle of 1/100 was calculated by the following expression:

$$f = \frac{r}{3 - 2 \cdot r} \tag{4.6}$$

where r is sheathing area ratio (Equation 3.1). It has been proposed that Equation 4.6 is applicable for prediction of capacity for typical light-frame shear walls.

Sugiyama and Matsumoto (1994) determined additional empirical equations (referred to as the W.U. equations) relating load and sheathing area ratio, based on all the tests performed for apparent shear deformation angles of 1/60, 1/100 and 1/300. These equations determine the shear load ratio at a particular apparent shear deformation angle.

For a shear deformation angles of 1/60 radians:

$$f = \frac{r}{2 - r} \tag{4.7}$$

For a shear deformation angle of 1/300 radians:

$$f = \frac{3 \cdot r}{8 - 5 \cdot r} \tag{4.8}$$

where f is shear load ratio and r is sheathing area ratio.

For an 8 ft. (2.4 m) high wall, shear deformation angles of 1/300, 1/100, and 1/60 correspond to racking displacements of 0.32 in. (8 mm), 0.96 in. (24 mm), and 1.6 in. (41 mm), respectively.

Predicted load resistance at a given interstory drift or at capacity of shear walls with openings is obtained by multiplying the shear load ratio, f, by the actual load resistance of the fully sheathed wall. However, the actual capacity is not known in design situations. For this reason, predictions determined from Equation 4.6 using the capacity of the fully sheathed wall determined in Section 5.6.1 as the reference capacity is also presented. As discussed in Section 5.6.1, the design stabilized capacity was determined as the ultimate design initial capacity multiplied by a reduction factor of 0.86.

Tables 5.8 and 5.9 compare actual load resistance at 0.32 in. (8 mm), 0.96 in. (24 mm), 1.6 in. (41 mm) and capacity with the predicted load resistance for the initial and stabilized cycles, respectively. Also included in Tables 5.8 and 5.9 are the actual and

predicted shear load ratios. The ratio of actual load resistance to predicted load resistance is included in Tables 5.8 and 5.9, where a ratio greater than 100% indicates a conservative prediction by Sugiyama's empirical equations and a ratio less than 100% indicates an unconservative prediction by Sugiyama's empirical equations.

As presented in Tables 5.8 and 5.9 and illustrated in Figure 5.23, the actual shear load ratios were higher than predicted by Equation 4.6 at capacity for all five walls. For the initial cycle, reserve capacity ranged from 24% to 88% for walls with openings when the actual fully sheathed capacity is used and 25% to 127% for the five shear walls when the design capacity is used as the reference capacity. For the stabilized cycle, reserve capacity ranged from 29% to 94% for walls with openings when the actual fully sheathed capacity is used and 7% to 100% for the five shear walls when the design capacity is used as the reference capacity. Wall specimens were stronger than predicted and Sugiyama's empirical equations conservatively predict cyclic capacity when the respective cyclic capacity for a fully sheathed wall is used as the base capacity. As with monotonic predictions at capacity, the percentage of reserve capacity increases as the amount of openings increases. Equation 4.6 tends to be overly conservative for walls with large openings.

For prediction at an interstory drift of 0.32 in. (8 mm), it is shown in Table 5.8 that Equation 4.8 made conservative predictions for 3 of the 4 walls with openings for the initial cycle. The predicted load of Wall C was 98% of the actual initial cycle load resistance. The reserve capacity of Walls B and D ranged from 6% to 12% and the reserve capacity of Wall E was 64%. For Walls A-D, predictions made by Equation 4.8 at 0.32 in. (8 mm) drift do not become overly conservative. As shown in Table 5.9, similar trends are found for the stabilized cycle.

Prediction made at 0.96 in. (24 mm) drift with Equation 4.6 are given in Tables 5.8 and 5.9. Initial cycle reserve capacities for walls with openings increased as the sheathing area ratio decreased and ranged from 17% to 73%. Stabilized cycle reserve capacities ranged from 18% to 77%. Similar to predictions at capacity, predictions at 0.96 in. (24 mm) become overly conservative as the percentage of openings increased.

At 1.6 in. (41 mm), Equation 4.7 was used to predict load resistance. As presented in Tables 5.8 and 5.9, reserve capacities ranged from 3% to 33% for the initial cycle and 2% to 33% for the stabilized cycle. The reserve capacities using Equation 4.7 do not tend to become overly conservative with opening size.

The use of Sugiyama's empirical equations have been applied to stiffness prediction at an interstory drift of 0.32 in. (8 mm). The predicted load resistance at 0.32 in. (8 mm) drift, determined using Equation 4.8, is divided by 0.32 in. (8 mm) to determine to predicted stiffness. Equation 4.6 was also used to predict load resistance at 0.32 in. (8 mm) and elastic stiffness. At this drift, Figures 5.5 and 5.6 show that the five wall configurations were behaving almost elastically. However, it is noted that drift corresponding to 40% of capacity ranged between 0.15 in. (4 mm) to 0.25 in. (6 mm),

Table 5. 8: Comparison of initial capacity of the five shear wall configurations examined with Sugiyama's predicted capacities

	Wall A	Wall B	Wall C	Wall D	Wall E
Initial Cycle	r = 1.0	r =0.76	r =0.55	r =0.48	r =0.30
Actual Capacity (kips)	32.0	20.3	13.6	11.5	7.5
Actual Shear Load Ratio	1.0	0.63	0.43	0.36	0.23
Eqn (4.6) Shear Load Ratio, f	1.0	0.51	0.29	0.24	0.13
Eqn (4.6) Predicted Capacity (kips) with Actual Capacity as reference	32.0	16.3	9.3	7.7	4.2
Actual Capacity/ Eqn (4.6) Prediction with Actual Capacity as reference	100%	124%	148%	150%	177%
Eqn (4.6) Predicted Capacity (kips) with 1994 UBC Capacity as reference	25.7	13.1	7.5	6.2	3.3
Actual Capacity / Eqn (4.6) Prediction with 1994 UBC Capacity as reference	125%	155%	181%	185%	227%
@0.32 in. drift (γ = 1/300)					
Actual Load (kips)	20.0	12.1	6.1	5.5	4.6
Predicted Load (kips) (Eqn 4.8)	20.0	10.8	6.2	5.2	2.8
Actual Shear Load Ratio	1.0	0.61	0.31	0.28	0.23
Eqn 4.8 Shear Load Ratio, f	1.0	0.54	0.31	0.26	0.14
Actual/Eqn (4.8) Shear Load Ratio	100%	112%	98%	106%	164%
@0.96 in. drift (γ = 1/100)					
Actual Load (kips)	31.7	19.0	11.8	10.9	7.1
Predicted Load (kips) (Eqn 4.6)	31.7	16.2	9.2	7.6	4.1
Actual Shear Load Ratio	1.0	0.60	0.37	0.34	0.22
Eqn 4.6 Shear Load Ratio, f	1.0	0.51	0.29	0.24	0.13
Actual/Eqn (4.6) Shear Load Ratio	100%	117%	128%	143%	173%
@1.6 in. drift (γ = 1/100)					
Actual Load (kips)	30.6	19.3	13.4	10.8	7.3
Predicted Load (kips) (Eqn 4.7)	30.6	18.7	11.6	9.8	5.5
Actual Shear Load Ratio	1.0	0.63	0.44	0.35	0.24
Eqn 4.7 Shear Load Ratio, f	1.0	0.61	0.38	0.32	0.18
Actual/Eqn (4.7) Shear Load Ratio	100%	103%	116%	110%	133%

Table 5. 9: Comparison of stabilized capacity of the five shear wall configurations examined with Sugiyama's predicted capacities

Stabilized Cycle	Wall A r = 1.0	Wall B r =0.76	Wall C r =0.55	Wall D r =0.48	Wall E r =0.30
Actual Capacity (kips)	27.5	17.4	11.8	9.9	6.6
Actual Shear Load Ratio	1.0	0.63	0.43	0.36	0.24
Eqn (4.6) Shear Load Ratio, f	1.0	0.51	0.29	0.24	0.13
Eqn (4.6) Predicted Capacity (kips) with Actual Capacity as reference	27.5	14.0	8.0	6.6	3.6
Actual Capacity/ Eqn (4.6) Prediction with Actual Capacity as reference	100%	124%	148%	150%	185%
Eqn (4.6) Predicted Capacity (kips) with Reduced 1994 UBC Capacity as reference	25.7	13.1	7.5	6.2	3.3
Actual Capacity / Eqn (4.6) Prediction with Reduced 1994 UBC Capacity as reference	107%	133%	157%	160%	200%
@0.32 in. drift (γ = 1/300)					
Actual Load (kips)	18.9	10.7	5.9	5.5	4.2
Predicted Load (kips) (Eqn 4.8)	18.9	10.2	5.9	4.9	2.6
Actual Shear Load Ratio	1.0	0.57	0.31	0.29	0.22
Eqn 4.8 Shear Load Ratio, f	1.0	0.54	0.31	0.26	0.14
Actual/Eqn (4.8) Shear Load Ratio	100%	106%	100%	112%	157%
@0.96 in. drift (γ = 1/100)					
Actual Load (kips)	27.2	16.4	10.9	9.5	6.3
Predicted Load (kips) (Eqn 4.6)	27.2	13.9	7.9	6.5	3.5
Actual Shear Load Ratio	1.0	0.60	0.40	0.35	0.23
Eqn 4.6 Shear Load Ratio, f	1.0	0.51	0.29	0.24	0.13
Actual/Eqn (4.6) Shear Load Ratio	100%	118%	138%	146%	177%
@1.6 in. drift (γ = 1/100)					
Actual Load (kips)	26.5	16.6	11.8	9.6	6.4
Predicted Load (kips) (Eqn 4.7)	26.5	16.2	10.1	8.5	4.8
Actual Shear Load Ratio	1.0	0.63	0.45	0.36	0.24
Eqn 4.7 Shear Load Ratio, f	1.0	0.61	0.38	0.32	0.18
Actual/Eqn (4.7) Shear Load Ratio	100%	102%	117%	113%	133%

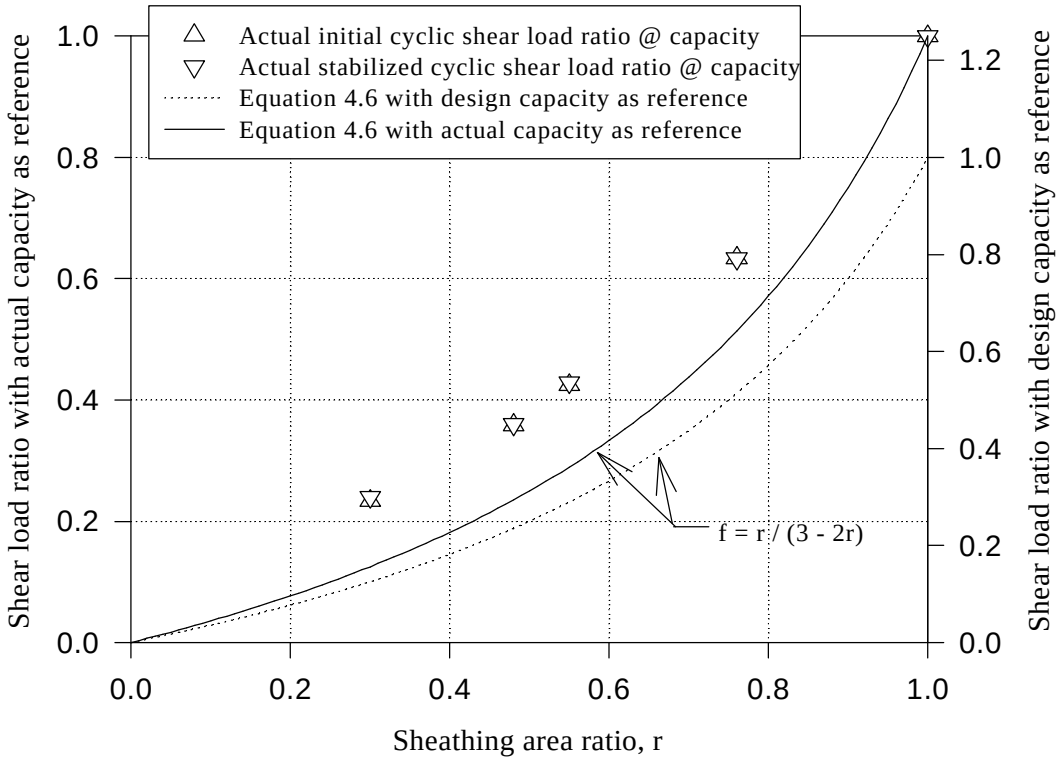

Figure 5. 23- Initial and stabilized shear load ratios of the five shear wall configurations examined, and Sugiyama's shear load ratio prediction equation plotted against sheathing area ratio

so slightly lower stiffness' would be expected when determined as the secant stiffness corresponding to 0.32 in. (8 mm) drift.

The predicted elastic stiffness' are compared in Tables 5.9 and 5.10. For the initial cycle, predicted elastic stiffness ranged from 8.1 kips/in (1400 kN/m) to 62.5 kips/in (10900 kN/m) when Equation 4.6 is used, and the actual stiffness was 12% to 25% higher than predicted for Walls A - D. The ratio of actual to predicted elastic stiffness for Wall E was 225%. For the stabilized cycle with Equation 4.6, actual elastic stiffness was 17% to 39% higher than predicted for Walls A - D. Again, the actual elastic stiffness was much higher than predicted.

Using Equation 4.8, predicted elastic stiffness ranged from 8.8 kips/in (1500 kN/m) to 62.5 kips/in (10900 kN/m) for the initial cycle. The actual elastic stiffness of Walls A - D were 3% to 18% higher than predicted. The actual elastic stiffness of Wall E was 207% higher than predicted. For the stabilized cycle, actual elastic stiffness ranged from 8.1 kips/in (1400 kN/m) to 59.1 kips/in (10300 kN/m). For Walls A - D, actual elastic stiffness was 11% to 31% higher than predicted. Actual elastic stiffness of Wall E was 222% higher than predicted.

Equation 4.8 provided better predictions of elastic stiffness for Walls A - D than Equation 4.6. However, predicted stiffness from Equation 4.8 must be used caution.

When predicted stiffness is used to calculate estimated drifts, unconservative estimates of drifts are found (i.e. estimated drifts are lower than actual). When predicted stiffness is used to calculate estimated load, conservative load estimates are found (i.e. estimated load is higher than actual).

Table 5. 10: Comparison of initial cycle elastic stiffness of the five shear wall configurations examined with elastic stiffness determined from Sugiyama

Initial Cycle	Wall A r = 1.0	Wall B r = 0.76	Wall C r = 0.55	Wall D r = 0.48	Wall E r = 0.30
Actual Elastic Stiffness (kips/in)	69.7	40.0	19.9	18.1	18.2
Actual Stiffness Ratio	1.0	0.57	0.29	0.26	0.26
Actual Load Resistance @ 0.32 in.	20.0	12.1	6.1	5.5	4.6
Actual Load Ratio @ 0.32 in.	1.0	0.61	0.31	0.28	0.23
Load Resistance Predicted @ 0.32 in. (kips) (Eqn 4.6)	20.0	10.2	5.8	4.8	2.6
Predicted Stiffness (kips/in) (=predicted load/ 0.32 in.)	62.5	31.9	18.1	15.0	8.1
Actual Stiffness / Predicted Stiffness	112%	125%	110%	120%	225%
Load Resistance Predicted @ 0.32 in. (kips/in) (Eqn 4.8)	20.0	10.8	6.2	5.2	2.8
Predicted Stiffness (kips/in) (=predicted load/ 0.32 in.)	62.5	33.8	19.4	16.2	8.8
Actual / Predicted Stiffness	111%	118%	103%	112%	207%

5.5.3 Natural Log Method

Predictions made by Sugiyama's empirical equations for cyclic loading were conservative for all five wall configurations, but the reserve strength was as high as 127%. Predictions which yield closer to the actual capacity are desirable for both design and analysis of shear walls.

The method of prediction presented here for shear walls with openings and tie-down anchorage at the extreme ends of the wall is referred to as the natural log method and is based on capacity data from the five shear walls examined. The natural log method process presented in the Section 4.4.3 is applied to the cyclic data and is explained again here. The natural log of the capacities of the five shear walls were plotted against sheathing area ratio, and a linear regression was found to fit the data well. Keeping the slope constant, the natural log method adjusts the y-intercept of the best

fit linear regression so that the equation predicts the capacity of the fully sheathed wall condition determined from current design methodology with conservative load factors.

Table 5. 11: Comparison of stabilized cycle elastic stiffness of the five shear wall configurations examined with elastic stiffness determined from Sugiyama

Stabilized Cycle	Wall A r = 1.0	Wall B r = 0.76	Wall C r = 0.55	Wall D r = 0.48	Wall E r = 0.30
Actual Elastic Stiffness (kips/in)	69.2	41.8	20.3	18.2	18.0
Actual Stiffness Ratio	1.0	0.60	0.29	0.26	0.26
Actual Load Resistance @ 0.32 in. (kips)	18.9	10.7	5.9	5.5	4.2
Actual Load Ratio @ 0.32 in.	1.0	0.57	0.31	0.29	0.22
Load Resistance Predicted @ 0.32 in. (kips) (Eqn 4.6)	18.9	9.6	5.5	4.5	2.5
Predicted Stiffness (kips/in) (=predicted load/ 0.32 in.)	59.1	30.0	17.2	14.1	7.8
Actual Stiffness / Predicted Stiffness	117%	139%	118%	129%	231%
Load Resistance Predicted @ 0.32 in. (kips/in) (Eqn 4.8)	18.9	10.2	5.9	4.9	2.6
Predicted Stiffness (kips/in) (=predicted load/ 0.32 in.)	59.1	31.9	18.3	15.4	8.1
Actual / Predicted Stiffness	117%	131%	111%	118%	222%

Figures 5.24 and 5.25 plot both natural log of capacity, F_{max}, and actual shear load ratios, f, determined for each wall during the initial and stabilized cycle against sheathing area ratio. Figures 5.24 and 5.25 also include the best fit regression equations and the natural log method prediction equation. For initial cycle, the natural log method prediction equations, with a reference capacity of 25.7 kips (kN), are:

$$LN(F_{max}) = 1.196 + 2.05 \cdot r \qquad (5.5a)$$

$$LN(f) = -2.05 + 2.05 \cdot r \qquad (5.5b)$$

For the stabilized cycle, the natural log method prediction equations, with a reference capacity of 25.7 kips (kN), are:

$$LN(F_{max}) = 1.226 + 2.02 \cdot r \quad (5.6a)$$

$$LN(f) = -2.02 + 2.02 \cdot r \quad (5.6b)$$

where F_{max} is capacity, f is shear load ratio, and r is sheathing area ratio.

Table 5.12 tabulates the initial and stabilized capacity of each wall with capacity determined from Equations 5.5a and 5.6a. The ratio of actual initial capacity to capacity determined from the natural log method fell in the range of 123% to 133%. The ratio of actual stabilized capacity to capacity from the best fit regression of the natural log of capacity fell in the range of 106% to 113%. For the five shear walls examined, the natural log method yields close, yet conservative capacity predictions of shear walls with openings and tie-down anchorage at the ends of the wall only.

Unlike Sugiyama's predictions, application of a uniform safety factor can be used regardless of the amount of openings, giving each wall the same percent reserve strength. Equations 5.5a and 5.5b can be solved for F_{max} and if:

$$F_{max} = e^{(1.196+2.05 \cdot r)} \quad (5.5c)$$

$$f = e^{(-2.05+2.05 \cdot r)} \quad (5.5d)$$

Then if a safety of factor of 3.0 is desired, the design value would be,

$$F_{design} = \frac{F_{max}}{3.0} = \frac{e^{(1.196+2.05 \cdot r)}}{3.0} \quad (5.5e$$

$$f_{design} = \frac{f}{3.0} = \frac{e^{(-2.05+2.05 \cdot r)}}{3.0} \quad (5.5f)$$

where F_{design} is the allowable shear value, F_{max} is the ultimate shear capacity, f_{design} is the allowable shear load factor, and f is the shear load ratio. Equation 5.5f can be used to predict the allowable initial cycle capacity by multiplying the strength ratio by the ultimate strength of a fully sheathed wall and ensure a uniform factor of safety. A similar process can be done based on the stabilized cycle.

The same methodology used to determine capacity estimates with the natural log method can be applied to predict elastic stiffness. There is one drawback to stiffness prediction, and that is there is not a design elastic stiffness to use as a reference. Figure 5.26 and 5.27 plot the natural log of elastic stiffness against sheathing area ratio. The best fit regression was a closer fit when Wall E was excluded, so a higher lower limit on sheathing area ratio of r = 0.48 was used for elastic stiffness estimates. The natural log best fit equation for initial cycle elastic stiffness, given in Figure 5.26, is:

$$LN(k_e) = 1.574 + 2.70 \cdot r \quad (5.7)$$

$$LN(k_e) = 1.605 + 2.68 \cdot r \quad (5.8)$$

where k_e is elastic stiffness and r is sheathing area ratio.

From Table 5.13, the actual to predicted ratio ranged from 93% to 106% for the initial cycle and 94% to 109% for the stabilized cycle. These are good estimates of elastic stiffness, but more data needs to be applied to the natural log method to determine its validity for a larger range of shear walls.

The applicability of prediction based on the natural log of capacity done in this research is limited, due to the small number of variables examined. However, a linear empirical equation predicting the natural log of capacity based on framing, sheathing, sheathing nailing, tie-down anchorage and openings potentially can be determined with more shear wall tests examining more of the variables found in typical shear wall construction.

5.6 Conclusions

The data from the monotonic shear wall tests has been presented and the following conclusions were drawn:

- Sheathing above and below openings resists shear
- Slip of nailed tie-down anchorage, relative to the ends studs, did not occur
- Gypsum sheathing was observed to fail after repetitive cycles at low displacement levels, leaving only plywood sheathing to resist shear
- Fatigue of plywood sheathing nailing was the predominant cause of failure
- Sugiyama's capacity predictions of shear walls with openings and tie-down anchorage at the ends of the wall only was conservative for all five wall configurations. However, this method was found to be overly conservative as the area of openings increased.
- Elastic stiffness prediction was found to overestimate actual elastic stiffness.
- The natural log method was found to provide good estimation of capacity forshear walls with openings and tie-down anchorage at the ends of the wall only.
- This method provides a more uniform conservatism to the design of walls with respect to sheathing area ratio. The natural log method is based on limited data and further cyclic tests of shear walls with openings needs to be performed to validate this prediction method.

5.7 Summary

The results of the five shear wall configurations when tested according to the definitions of sequential phased displacement loading has been presented and discussed. Current design methodology has been compared with actual capacity, and two conservative methods of prediction have been presented.

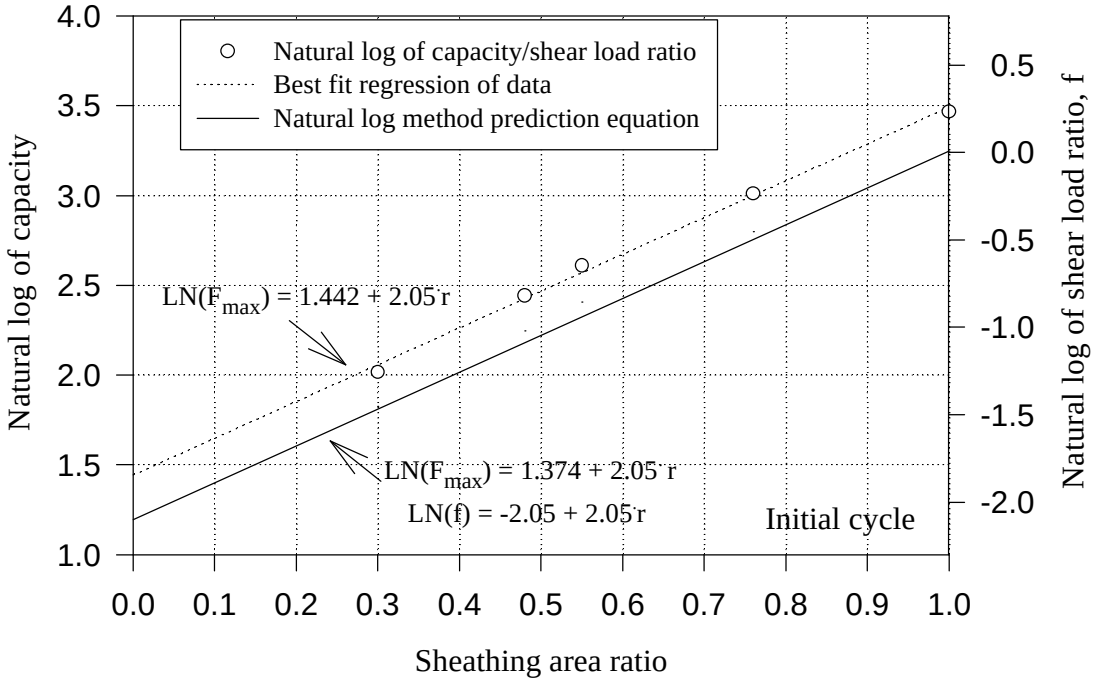

Figure 5. 24- Natural log of initial capacity of the five shear wall configurations examined, and natural log method prediction equation plotted against sheathing area ratio

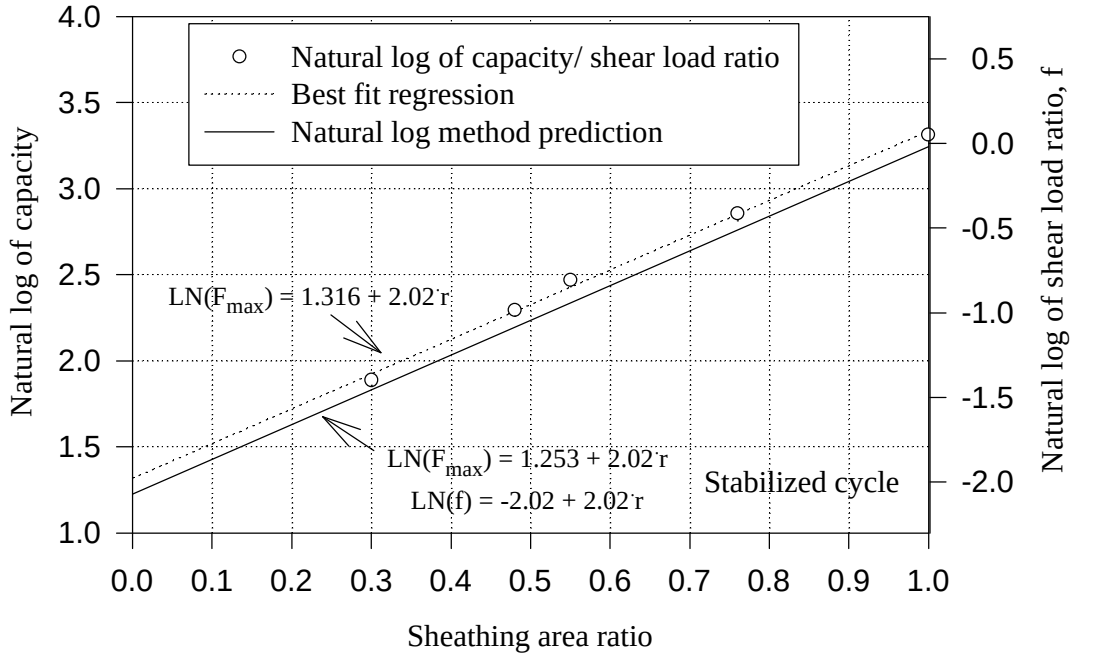

Figure 5. 25 - Natural log of stabilized capacity of the five shear wall configurations examined, and natural log method prediction equation plotted against sheathing area ratio

Table 5. 12: Comparison of initial and stabilized capacity of the five shear wall configurations examined with natural log method predicted capacities

	Wall A	Wall B	Wall C	Wall D	Wall E
	r = 1.0	r = 0.76	r =0.55	r = 0.48	r = 0.30
Initial cycle:					
actual F_{max}	32.0	20.3	13.6	11.5	7.5
predicted F_{max}	25.7	15.7	10.2	8.8	6.1
Actual/ predicted F_{max}	125%	129%	133%	131%	123%
Stabilized cycle:					
actual F_{max}	27.5	17.4	11.8	9.9	6.6
predicted F_{max}	25.7	15.8	10.4	9.0	6.2
actual/ predicted F_{max}	107%	110%	113%	110%	106%

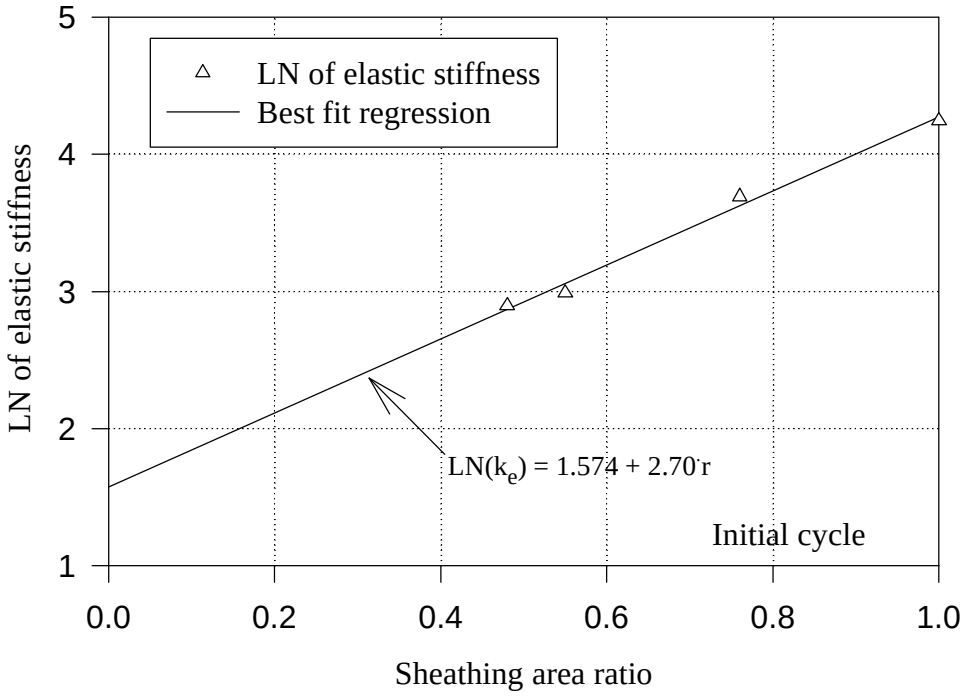

Figure 5. 26 - Natural log of initial elastic stiffness of Walls A - D, and natural log method prediction equation plotted against sheathing area ratio

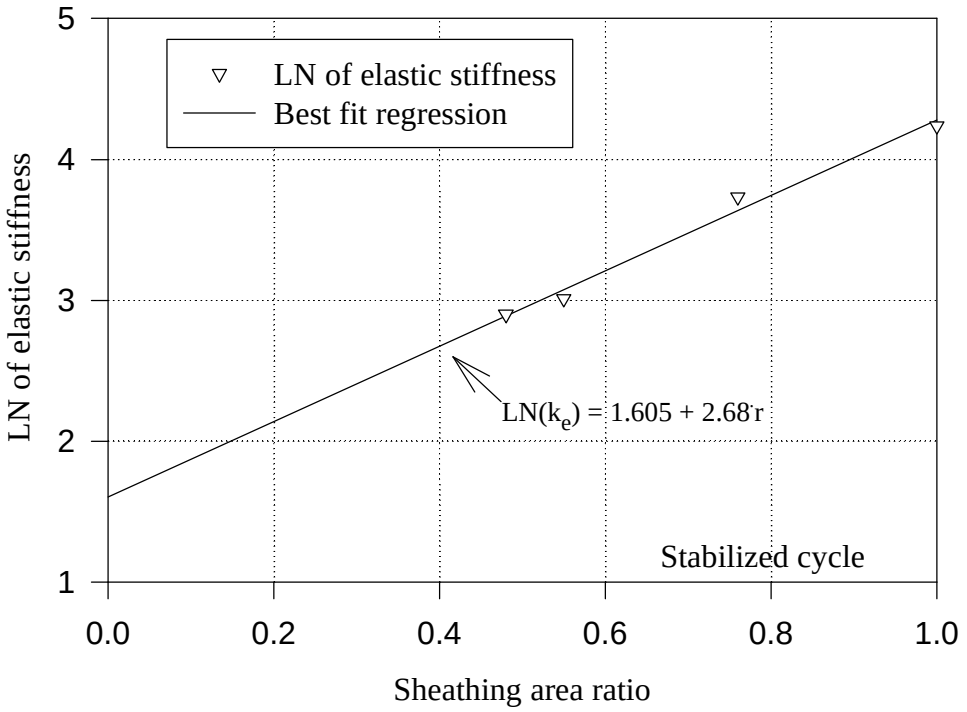

Figure 5. 27 - Natural log of stabilized elastic stiffness of Walls A - D, and natural log method prediction equation plotted against sheathing area ratio

Table 5. 13: Comparison of initial and stabilized capacity of the five shear wall configurations examined with natural log method predicted capacities

	Wall A r = 1.0	Wall B r = 0.76	Wall C r =0.55	Wall D r = 0.48
Initial cycle:				
actual elastic stiffness	69.7	40.0	19.9	18.1
predicted elastic stiffness	71.8	37.6	21.3	17.6
Actual/ predicted elastic stiffness	0.97	1.06	0.93	1.03
Stabilized cycle:				
actual elastic stiffness	69.2	41.8	20.3	18.2
predicted elastic stiffness	72.6	38.2	21.7	18.0
Actual/ predicted elastic stiffness	0.95	1.09	0.94	1.01